Chemical Science



MINIREVIEW

View Article Online
View Journal | View Issue



Cite this: *Chem. Sci.*, 2018, **9**, 6017

All publication charges for this article have been paid for by the Royal Society of Chemistry

# Mechanisms of catalytic reduction of $CO_2$ with heme and nonheme metal complexes

Shunichi Fukuzumi, *[ab] Yong-Min Lee, *[ac] Hyun S. Ahn *[d] and Wonwoo Nam *[ae]

The catalytic conversion of $CO_2$ into valuable chemicals and fuels has attracted increasing attention, providing a promising route for mitigating the greenhouse effect of $CO_2$ and also meeting the global energy demand. Among many homogeneous and heterogeneous catalysts for $CO_2$ reduction, this minireview is focused on heme and nonheme metal complexes that act as effective catalysts for the electrocatalytic and photocatalytic reduction of $CO_2$. Because metalloporphyrinoids show strong absorption in the visible region, which is sensitive to the oxidation states of the metals and ligands, they are suited for the detection of reactive intermediates in the catalytic $CO_2$ reduction cycle by electronic absorption spectroscopy. The first part of this review deals with the catalytic mechanism for the one-electron reduction of $CO_2$ to oxalic acid with heme and nonheme metal complexes, with an emphasis on how the formation of highly energetic $CO_2^{\bullet-}$ is avoided. Then, the catalytic mechanism of two-electron reduction of $CO_2$ to produce CO and $H_2O$ is compared with that to produce HCOOH. The effect of metals and ligands of the heme and nonheme complexes on the CO or HCOOH product selectivity is also discussed. The catalytic mechanisms of multi-electron reduction of $CO_2$ to methanol (six-electron reduced product) and methane (eight-electron reduced product) are also discussed for both electrocatalytic and photocatalytic systems.

Received 19th May 2018
Accepted 26th June 2018

DOI: 10.1039/c8sc02220h

rsc.li/chemical-science

[a]*Department of Chemistry and Nano Science, Ewha Womans University, Seoul 03760, Korea. E-mail: fukuzumi@chem.eng.osaka-u.ac.jp; yomlee@ewha.ac.kr; wwnam@ewha.ac.kr*

[b]*Graduate School of Science and Engineering, Meijo University, Nagoya, Aichi 468-8502, Japan*

[c]*Research Institute for Basic Sciences, Ewha Womans University, Seoul 03760, Korea*

[d]*Department of Chemistry, Yonsei University, Seoul 03722, Korea. E-mail: ahnhs@yonsei.ac.kr*

[e]*School of Chemistry and Chemical Engineering, Shaanxi Normal University, Xi'an 710119, P. R. China*

*Shunichi Fukuzumi earned a bachelor's degree and a Ph.D. degree in applied chemistry from the Tokyo Institute of Technology in 1973 and 1978, respectively. After working as a postdoctoral fellow from 1978 to 1981 at Indiana University in USA, he became an Assistant Professor in 1981 at Osaka University where he was promoted to a Full Professor in 1994. His research has been focused on electron transfer chemistry, particularly artificial photosynthesis. He is currently a Distinguished Professor at Ewha Womans University, a Designated Professor at Meijo University, and a Professor Emeritus at Osaka University.*

*Yong-Min Lee received his M.S. and Ph.D. degrees in Inorganic Chemistry from Pusan National University, Republic of Korea, under the supervision of Professor Sung-Nak Choi in 1999. After he worked at the Magnetic Resonance Centre (CERM) at the University of Florence, Italy, as a Postdoctoral fellow and Researcher under the direction of Professors Ivano Bertini and Claudio Luchinat from 1999 to 2005, he joined the Centre for Biomimetic Systems at Ewha Womans University, as a Research Professor in 2006. He is currently a Special Appointment Professor at Ewha Womans University since 2009.*

## 1 Introduction

Solar-driven reduction of $CO_2$ has merited increasing attention due to the hike in the world-wide consumption of fossil fuels and the consequential escalation in the atmospheric $CO_2$ level.[1–9] There have so far been extensive studies on solar-driven reduction of $CO_2$ (ref. 7–21) as well as electrocatalytic reduction[22–36] and catalytic hydrogenation of $CO_2$ in aprotic solvents and also in water.[37–51] Carbon dioxide can be reduced by one electron and one proton to produce a half equivalent of oxalic acid ($H_2C_2O_4$) with a standard reduction potential of −0.50 V *vs.* SHE [eqn (1)].[26,52] The two-electron reduction of $CO_2$ with two protons affords formic acid (HCOOH) [eqn (2)] or CO and $H_2O$ [eqn (3)] with the standard reduction potentials of −0.25 and −0.11 V, respectively.[52] Carbon dioxide can be further reduced by four, six, and eight electrons with four, six, and eight protons to produce formaldehyde [HCHO: eqn (4)], methanol [$CH_3OH$: eqn (5)] or ethylene [$C_2H_4$: eqn (6)], and methane [$CH_4$: eqn (7)] with the standard reduction potentials of −0.07, +0.02 or +0.06 V, and +0.17 *vs.* SHE, respectively.[52] Therefore, the standard reduction potential is anodically shifted with an increased number of electrons and protons for $CO_2$ reduction, indicating that the involvement of a higher number of electrons and protons favours the $CO_2$ reduction thermodynamically. However, because the kinetic barrier generally increases with an additional number of electrons and protons involved in the reaction, appropriate catalysts are required to facilitate turnovers.

$$CO_2 + e^- + H^+ \rightarrow (1/2)H_2C_2O_4,\ E^0 = -0.50\ \text{V}\ \textit{vs.}\ \text{SHE} \quad (1)$$

$$CO_2 + 2e^- + 2H^+ \rightarrow HCOOH,\ E^0 = -0.25\ \text{V}\ \textit{vs.}\ \text{SHE} \quad (2)$$

$$CO_2 + 2e^- + 2H^+ \rightarrow CO + H_2O,\ E^0 = -0.11\ \text{V}\ \textit{vs.}\ \text{SHE} \quad (3)$$

$$CO_2 + 4e^- + 4H^+ \rightarrow HCHO + H_2O,\ E^0 = -0.07\ \text{V}\ \textit{vs.}\ \text{SHE} \quad (4)$$

$$CO_2 + 6e^- + 6H^+ \rightarrow CH_3OH + H_2O,\ E^0 = +0.02\ \text{V}\ \textit{vs.}\ \text{SHE} \quad (5)$$

$$CO_2 + 6e^- + 6H^+ \rightarrow (1/2)C_2H_4 + 4H_2O,\ E^0 = +0.06\ \text{V}\ \textit{vs.}\ \text{SHE} \quad (6)$$

$$CO_2 + 8e^- + 8H^+ \rightarrow CH_4 + 2H_2O,\ E^0 = +0.17\ \text{V}\ \textit{vs.}\ \text{SHE} \quad (7)$$

Among many catalysts for $CO_2$ reduction, metalloporphyrinoid complexes are suitable for mechanistic studies, because metalloporphyrinoids such as heme have intense absorption bands, which are sensitive to the oxidation states of metals and porphyrinoid ligands.[53–58] Not only heme but also nonheme metal complexes have merited significant interest as bioinspired catalysts, which are studied in many redox reactions.[26,58–73] This review is intended to focus on the mechanisms of both electrocatalytic and photocatalytic reduction of $CO_2$ with heme and nonheme metal complexes. The catalytic mechanisms are discussed not only for the one-electron/one-proton and two-electron/two-proton reductions of $CO_2$ [eqn (1) and (3)] but also for multi-electron/multi-proton pathways [eqn (4)–(7)]. The electrocatalytic and photocatalytic efficiencies are discussed based on the overpotentials and quantum yields, respectively.

## 2 Catalytic one-electron reduction of $CO_2$ to oxalic acid

The standard one electron reduction potential of $CO_2$ to $CO_2^{\bullet}$ is as negative as −2.21 V *vs.* SCE (=−1.97 V *vs.* SHE) in *N*,*N*′-dimethylformamide (DMF)[74] and −1.90 V *vs.* SCE in water.[75] The dimerization of $CO_2^{\bullet}$ affords oxalate dianions ($C_2O_4^{2-}$).[76] Therefore, catalysts are required to avoid the formation of highly energetic $CO_2^{\bullet}$ and secure a low energy pathway en route to oxalic acid.

$Ag^{II}$ and $Pd^{II}$ complexes of both 2,3,7,8,12,13,17,18-octaethylporphyrin (OEP) and 5,10,15,20-tetraphenylporphyrin (TPP) were reported to act as catalysts for one-electron reduction of $CO_2$ to produce oxalic acid in $CH_2Cl_2$ containing 0.10 M tetrabutylammonium fluoride (TBAF) at an applied potential of −1.65 and −1.80 V *vs.* SCE, respectively.[77] In comparison with

*Hyun S. Ahn earned his undergraduate degrees in chemistry and chemical engineering from the University of Washington in Seattle (2008). He then pursued his Ph.D. studies at the University of California at Berkeley, in the field of inorganic chemistry under the supervision of Prof. T. Don Tilley. Upon conferral of his Ph.D. in 2013, Hyun continued his research as a postdoctoral scholar at the University of Texas at Austin with Prof. Allen J. Bard. He is currently an assistant professor of chemistry at Yonsei University. Hyun's research interest spans across the fields of catalysis, photoelectrochemistry, bio-electrochemistry, and energy conversion technologies.*

*Wonwoo Nam earned his B.S. (Honours) degree in Chemistry from California State University, Los Angeles, and his Ph.D. degree in Inorganic Chemistry from the University of California, Los Angeles (UCLA) under the supervision of Professor Joan S. Valentine in 1990. After working as a postdoctoral fellow at UCLA for one year, he became an Assistant Professor at Hong Ik University in 1991. In 1994, he moved to Ewha Womans University, where he is currently a Distinguished Professor. His current research has been focused on the dioxygen activation, water oxidation, and important roles of metal ions in bioinorganic chemistry.*

$Ag^{II}$(TPP) and $Pd^{II}$(TPP), neither $Cu^{II}$(TPP) nor $Ni^{II}$(TPP) showed catalytic activity for the electrochemical $CO_2$ reduction.[77]

In contrast to $Cu^{II}$(TPP), a dinuclear nonheme copper(II) complex ($[\mathbf{4}]^{4+}$) can catalyse the one-electron reduction of $CO_2$ in acetonitrile (MeCN) in the presence of $LiClO_4$ to produce lithium oxalate at an applied potential of −0.03 V *vs.* NHE.[78] The electrochemical reduction of $[\mathbf{4}]^{4+}$ at a cathodic peak potential ($E_{pc}$) of +0.06 V *vs.* NHE (=+0.06 V *vs.* SHE) produced a dinuclear copper(I) complex ($[\mathbf{1}]^{2+}$) that is oxidized in air selectively by $CO_2$ (rather than $O_2$) to yield a tetranuclear copper(II) complex containing two bridging $CO_2$-derived oxalate groups ($[\mathbf{2}]^{4+}$) as shown in Scheme 1.[78] The treatment of the copper(II) oxalate complex in MeCN with a soluble lithium salt results in the quantitative precipitation of lithium oxalate.[78] DFT calculations suggest the catalytic mechanism (Scheme 2) in which one $CO_2$ molecule is first reduced cooperatively by two Cu(I) metals to give a fully delocalized mixed-valence $Cu^{I}/Cu^{II}(CO_2^{\bullet})$ radical anion intermediate, followed by further partial reduction of the metal-ligated $CO_2$ molecule and (metal-mediated) nucleophilic-like attack on the carbon atom of an incoming second $CO_2$ molecule to afford the dinuclear Cu(II)-oxalate product ($[\mathbf{2}]^{4+}$).[79]

A binuclear metallacyclic copper complex was reported to be capable of selectively capturing $CO_2$ from air and reduce $CO_2$ to oxalate, in the form of an oxalate-bridged complex. The oxalate-bridged complex releases oxalic acid when it is treated with dilute mineral acid to regenerate the original copper complex.[80]

It has also been reported that the one-electron reduction of chalcogen-bridged tricopper cyclophanates ($Cu_3EL$: $L^{3-}$ = tris(β-diketiminate; E = S, Se) (the one-electron reduction potential: $E_{red}$ = −0.89 and −1.04 V *vs.* SCE, respectively) by $CoCp_2^*$ (one-electron oxidation potential: $E_{ox}$ = −1.94 V *vs.* $Fc/Fc^+$), $FeCp(C_6Me_6)$ ($E_{ox}$ = −2.07 V *vs.* $Fc/Fc^+$), or $KC_8$ ($E_{ox}$ < −3.7 V *vs.* $Fc/Fc^+$) in the presence of $KPF_6$ in DMF afforded $[Cu_3EL]^-$, which reacts with $CO_2$ to yield exclusively $C_2O_4^{2-}$ (95% yield, TON = 24) and regenerate $Cu_3EL$.[81] Catalysis is observed employing $KC_8$ and $FeCp(C_6Me_6)$ as reductants, but only in the presence of $KPF_6$.[81]

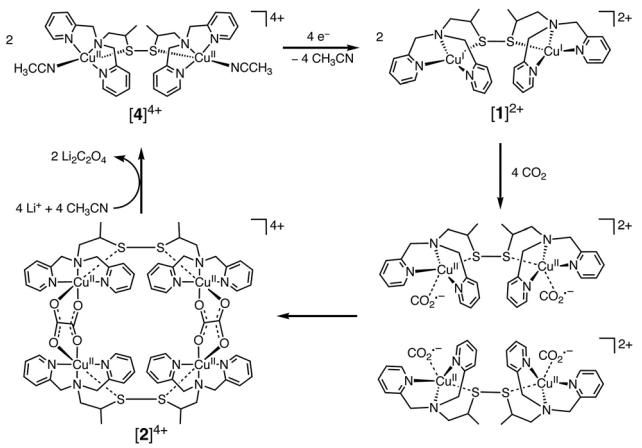


Scheme 1 Catalytic one-electron reduction of $CO_2$ to oxalate with a dinuclear copper(I) complex ($[\mathbf{1}]^{2+}$). Reprinted with permission from ref. 78. Copyright 2010, The American Association for the Advancement of Science.

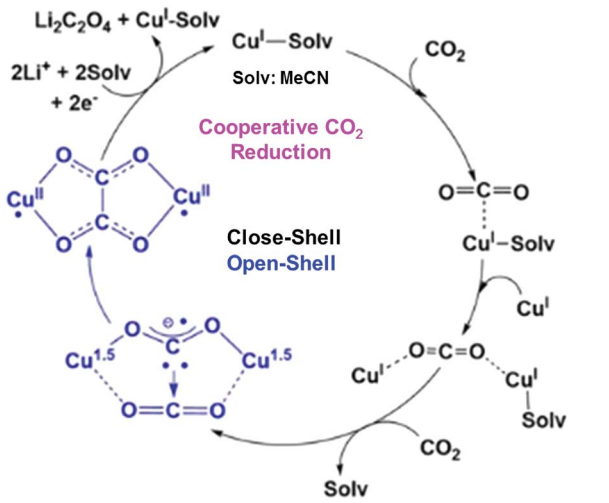


Scheme 2 Proposed catalytic cycle for one-electron reduction of $CO_2$ to oxalate with a copper(I) complex. Reprinted with permission from ref. 79. Copyright 2017, American Chemical Society.

## 3 Electrocatalytic reduction of $CO_2$ to CO with metalloporphyrins

Iron tetraphenylporphyrin [Fe(TPP)] (Fig. 1) was reported to catalyse the electrochemical reduction of $CO_2$ at the $Fe^{I}/Fe^{0}$ redox potential (−1.64 V *vs.* SCE) in DMF.[82] However, the catalytic efficiency was very low and the catalytic activity of Fe(TPP) was rapidly lost during preparative-scale electrolysis.[82] The addition of $Mg^{2+}$ ions to the solution resulted in improved catalytic efficiency, resulting in a CO faradaic yield of *ca.* 60–70% and the rest in formate.[83] The presence of Lewis acids, such as $Li^+$, $Na^+$, $Ba^{2+}$, and $Al^{3+}$ ions, also improved the catalytic efficiency. The addition of $CF_3CH_2OH$ (1.47 M) resulted in a large increase of the $Fe^{I}/Fe^{0}$ current to reach an $i_p/i_p^0$ value of 131.[82] The $i_p/i_p^0$ value is given by eqn (8),

$$i_p/i_p^0 = 2.24(k_{app}[CO_2]RT/Fv)^{1/2} \quad (8)$$

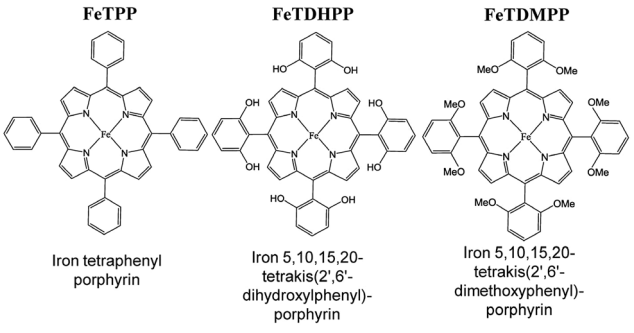


Fig. 1 Iron tetraphenylporphyrin derivatives used for electrocatalytic reduction of $CO_2$ to CO. Reprinted with permission from ref. 86. Copyright 2012, The American Association for the Advancement of Science.

where $k_{app}$ is the rate constant, $R$ is the gas constant, $T$ is the absolute temperature, $F$ is the Faraday constant, and $v$ is the scan rate.[83] The $i_p/i_p^0$ value was proportional to the concentration of $CF_3CH_2OH$ at low concentrations, indicating that $k_{app}$ exhibits second-order dependence on $[CF_3CH_2OH]$: $k_{app} \propto [CF_3CH_2OH]^2$.[83] Such second-order dependence of $k_{app}$ on $[CF_3CH_2OH]$ suggests that the rate-determining step in the electrocatalytic reduction of $CO_2$ to CO involves a two-step protonation of the $CO_2$ adduct of $[PFe^0]^{2-}$ ($[PFe^{II}CO_2]^{2-}$) by AH to produce $[PFe^{II}CO]$ with dehydration as shown in Scheme 3, where $AH = CF_3CH_2OH$.[83,84] The $CO_2$ adduct of an $Fe^0$ porphyrin ($[PFe^{II}CO_2]^{2-}$) was characterised by vibration at 590 $cm^{-1}$ and CO bending mode at 806 $cm^{-1}$, which are both sensitive to $^{13}C$ substitution.[85] The $[PFe^{II}CO_2]^{2-}$ complex, which could only be observed at −95 °C, was easily protonated by methanol even at −80 °C to produce $[PFe^{II}C(OH)O]^-$.[85]

The electrocatalytic efficiency of $CO_2$ reduction to CO was improved by the introduction of phenolic groups in all *ortho* and *ortho′* positions of the phenyl groups of iron tetraphenylporphyrin.[86] The electrocatalytic reduction of $CO_2$ with iron 5,10,15,20-tetrakis(2′,6′-dihydroxyphenyl)porphyrin (FeTDHPP in Fig. 1) in the presence of 2 M $H_2O$ in $CO_2$-saturated DMF ($[CO_2]$ = 0.23 M) afforded a CO faradaic yield of 94% with a turnover number (TON) of $5.0 \times 10^7$ for 4 hours of electrolysis at −1.16 V *vs.* SHE with no observed degradation.[86] The average current density was 0.31 mA $cm^{-2}$ that corresponds to a turnover frequency (TOF) of $3.2 \times 10^3$ $s^{-1}$ at an overpotential of 0.466 V, which is the most efficient among other $CO_2$ reduction catalysts.[86–90] When the hydroxy groups in FeTDHPP were replaced by methoxy groups (FeTDMPP in Fig. 1), the catalytic activity of FeTDMPP was decreased by a factor of around 1 billion as compared to that of FeTDHPP with hydroxyl groups.[86] Therefore, the enhanced catalytic activity of FeTDHPP was attributed to the high local concentration of protons associated with the phenolic hydroxy substituents.[86]

The introduction of four positively charged trimethylanilinium groups on the phenyl groups of iron tetraphenylporphyrin resulted in further improvement of the electrocatalytic activity of $CO_2$ reduction by means of coulombic stabilization of the initial $Fe^0$–$CO_2$ adduct.[88] When four positively charged trimethylanilinium groups were introduced at the *ortho* positions of the TPP groups (Fe-*o*-TMA in Fig. 2), the maximum TOF was as high as $10^6$ $s^{-1}$ at a low overpotential of 0.220 V.[88] The catalyst standard potential ($E^0_{cat}$) of Fe-*o*-TMA was determined to be −0.944 V *vs.* SHE, which is the most positive ever reported for an iron porphyrin $CO_2$-reduction catalyst.[88] The *para*-substituted analogue (Fe-*p*-TMA in Fig. 2) exhibited an $E^0_{cat}$ value of −1.263 V *vs.* SHE, which is much more negative than that of Fe-*o*-TMA, due to smaller coulombic stabilization of the initial $Fe^0$–$CO_2$ adduct.[88] The importance of the coulombic stabilization for the electrocatalytic activity of $CO_2$ reduction was further demonstrated by the introduction of four negatively charged sulfonate groups on the phenyl groups of iron tetraphenylporphyrin (Fe-*p*-PSULF in Fig. 2), which resulted in a more negative $E^0_{cat}$ value (−1.428 V *vs.* SHE).[88]

In contrast to the electrocatalytic reduction of $CO_2$ in nonaqueous aprotic solvents such as DMF (*vide supra*), the electrocatalytic reduction of $CO_2$ in water always competes with the reduction of aqueous protons to hydrogen ($H_2$). The TOF of the electrocatalytic $CO_2$ reduction in an aqueous solution was reported to be much smaller compared to that in DMF solution because of the lower solubility of $CO_2$ in water.[88] A successful example of selective electrocatalytic reduction of $CO_2$ to CO over proton reduction was reported by employing Fe-*p*-TMA (Fig. 2) as a catalyst. This preparative-scale electrolysis was performed in water at pH 6.7 (adjusted by KOH addition) with an applied potential of −0.97 V *vs.* NHE for 4 h.[88] The average faradaic yields were CO (90%), $H_2$ (7%), acetate (1.4%), formate (0.7%) and oxalate (0.5%).[88] When pH was adjusted to 3.7 by the addition of 0.1 M formic acid buffer, the electrolysis with Fe-*p*-TMA resulted in the exclusive proton reduction to produce $H_2$ over the $CO_2$ reduction.[88]

The selective electrocatalytic reduction of $CO_2$ to CO (over proton reduction) under acidic conditions was made possible with a cobalt(II) chlorin complex, $Co^{II}$(Ch), adsorbed on multi-walled carbon nanotubes (MWCNTs) as a catalyst (Fig. 3).[91]

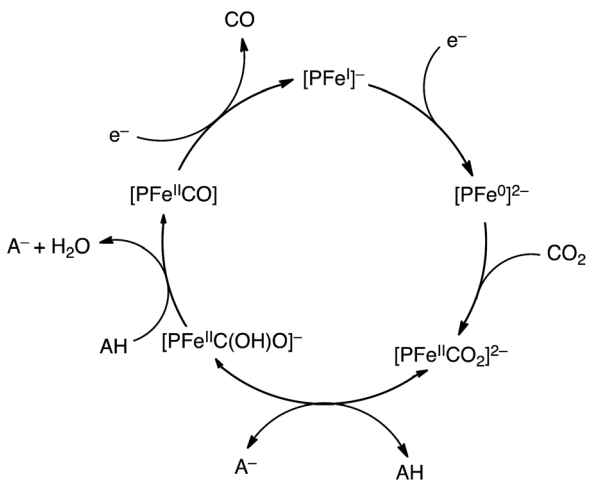


Scheme 3 Catalytic cycle for two-electron reduction of $CO_2$ to CO with an iron porphyrin ($[PFe^I]^-$).[84]

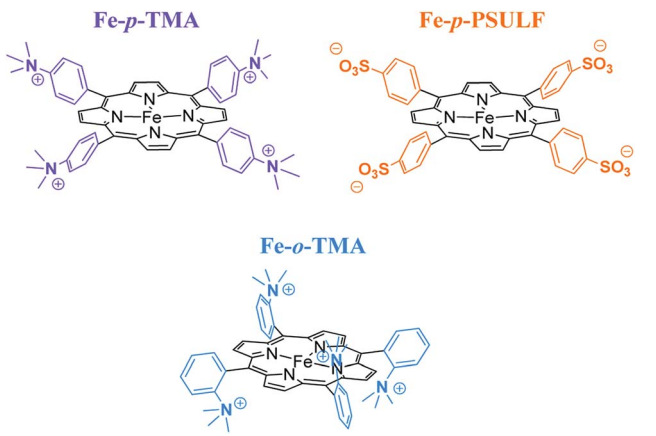


Fig. 2 Iron tetraphenylporphyrin derivatives with positive and negative charges used for electrocatalytic reduction of $CO_2$ to CO. Reprinted with permission from ref. 88. Copyright 2016, American Chemical Society.

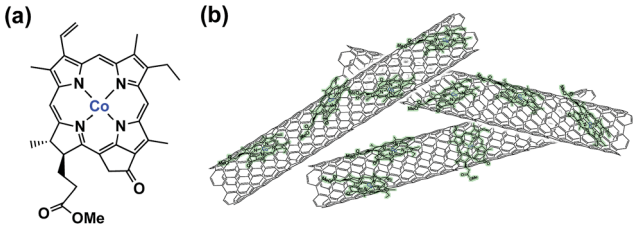


Fig. 3 (a) Structure of $Co^{II}$(Ch) and (b) schematic image of $Co^{II}$(Ch) on MWCNTs. Reprinted with permission from ref. 91. Copyright 2015, Royal Society of Chemistry.

The electrolysis of a $CO_2$-saturated aqueous solution (pH = 4.6 with $Na_2SO_4$) employing a glassy carbon working electrode modified with $Co^{II}$(Ch)@MWCNT (0.01 μmol) afforded mainly CO with a maximum TON of 1500 and TOF of 100 $h^{-1}$ and little $H_2$ at −1.1 V *vs.* NHE (=−1.34 V *vs.* SCE).[91] The faradaic yield of CO for the initial 2 h was determined to be as high as 89%, whereas that for $H_2$ production was only 11% at pH 4.6.[91] The high selectivity for CO was maintained at pH 3.6, although $H_2$ became the main product at pH 2.0.[91]

When MWCNTs were replaced by reduced graphene oxide (rGO), which is a planar π-system, as a support material of $Co^{II}$(Ch), the CO yield became significantly smaller (TON = 350 for CO and 250 for $H_2$ at 20 h) (Fig. 4b) compared to that with

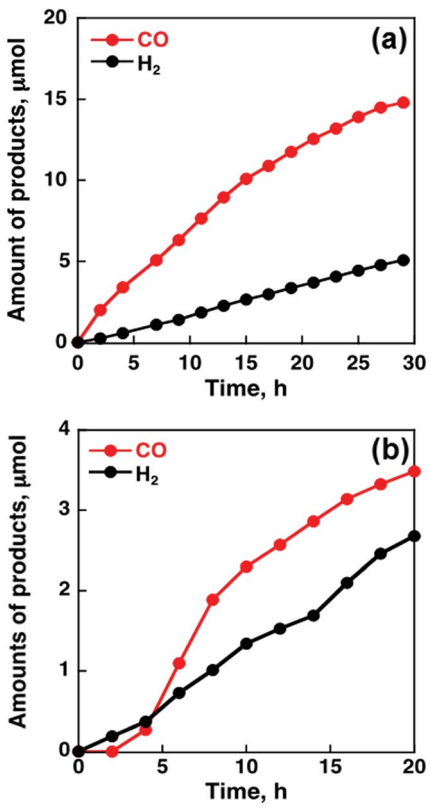


Fig. 4 Time profiles of the formation of CO and $H_2$ in the electrocatalytic reduction of $CO_2$ on a glassy carbon electrode modified with $Co^{II}$(Ch) (0.01 μmol) adsorbed on (a) MWCNTs (13 μg) and (b) rGO (13 μg) in a $CO_2$-saturated aqueous solution (pH 4.6) containing $Na_2SO_4$ (5.0 mM) at an applied potential of −1.34 V *vs.* SCE. Reprinted with permission from ref. 91. Copyright 2015, Royal Society of Chemistry.

MWCNTs (Fig. 4a).[91] Thus, the three dimensional assembly of MWCNTs with $Co^{II}$(Ch) (Fig. 3b) on the electrode surface is essential for the selective electrocatalytic reduction of $CO_2$ to CO.[91] The π–π interaction between MWCNTs and $Co^{II}$(Ch) is presumed to provide a suitable hydrophobic environment for more selective binding of $CO_2$ over protons compared to the system with two-dimensional rGO as a support material.[91]

FeTDHPP (Fig. 1), a known $CO_2$ reduction catalyst in DMF, also exhibits electrocatalysis in a $CO_2$-saturated aqueous solution (pH 7.3, $NaHCO_3$ 0.5 M) at an applied potential of −1.03 V *vs.* NHE ($\eta$ = 480 mV), selectively producing CO over $H_2$.[92] A surface immobilisation tactic was implemented for the FeTDHPP catalyst on carbon surfaces by removing one phenyl group and appending a pyrene unit through a short linker.[92] This immobilisation boosted both selectivity (96 : 4 CO : $H_2$ ratio) and overall conversion (97% total faradaic yield).[92]

The cobalt phthalocyanine (CoPc) complex when adsorbed on MWCNTs was demonstrated to be an electrocatalyst for $CO_2$ reduction to CO at −0.63 V *vs.* RHE, with a remarkable TON of $9.7 \times 10^4$ and a faradaic yield exceeding 90%.[93] Compared to CoPc/MWCNT (2.5%), CoPc/rGO (2.2%) and CoPc/CB (3.3%) (CB: carbon black) exhibited less than one-third of the current density at −0.59 V *vs.* RHE with a 10% lower faradaic yield of CO and inferior stability.[93] The higher graphitic nature of CNTs compared to those of either rGO or CB allows stronger π–π interactions with CoPc and higher electron conduction, resulting in superior electrocatalysis.[93] A Pc/CNT hybrid without Co afforded a much lower faradaic yield for CO (only 19%), indicating that the Co centres in the CoPc/CNT act as the primary catalyst active sites.[85] Low but non-zero conversion of $CO_2$ to CO on Pc/CNT is attributed to the catalytic activity of Pc itself.[93]

An iron tetraphenylporphyrin bearing six pendant OH groups in *ortho* and *ortho′* positions on three of the phenyl rings and one carboxylic acid group in the *para* position of the fourth phenyl was covalently attached to MWCNTs ($CATCO_2H$, Scheme 4).[94] The covalent grafting of an Fe porphyrin on MWCNTs also led to efficient electrocatalytic reduction of $CO_2$ to CO selectively in water (pH 7.3) at an overpotential of 0.5 V.[94]

Remarkably, the redox silent zinc(II) complex of 5,10,15,20-tetramesitylporphyrin (ZnTPP) was also reported as an effective electrocatalyst that afforded faradaic efficiencies as high as 95% for $CO_2$ reduction to CO at −1.7 V *vs.* SHE in DMF/$H_2O$ (9 : 1 v/v).[95] The UV-vis spectrum of the reduced ZnTPP species exhibits absorption bands at 710, 820, and 920 nm (Fig. 5, red line), which are the characteristic features of a transiently generated Zn complex with reduced ligands (*i.e.*, $TPP^{\bullet}$).[95] $ZnTPP^{\bullet}$ can react with $CO_2$ to regenerate ZnTPP and unidentified species.[95] The exact mechanism of the $CO_2$ reduction by $ZnTPP^{\bullet}$ is yet to be clarified.

## 4 Electrocatalytic reduction of $CO_2$ to CO with nonheme metal complexes

A nonheme cobalt complex with a macrocyclic aminopyridine (**I** in Scheme 5) can also catalyse the electrochemical reduction of $CO_2$ to CO with a faradaic efficiency of 98 ± 2% and 1.22(1)

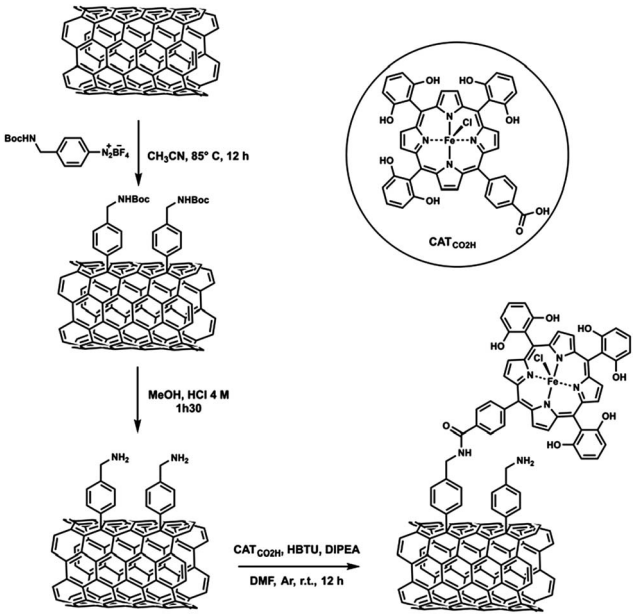


Scheme 4 An iron tetraphenylporphyrin bearing six pendant OH groups in *ortho* and *ortho′* positions on three of the phenyl rings and one carboxylic acid group in the *para* position of the fourth phenyl covalently attached to MWCNTs. Reprinted with permission from ref. 94. Copyright 2016, Royal Society of Chemistry.

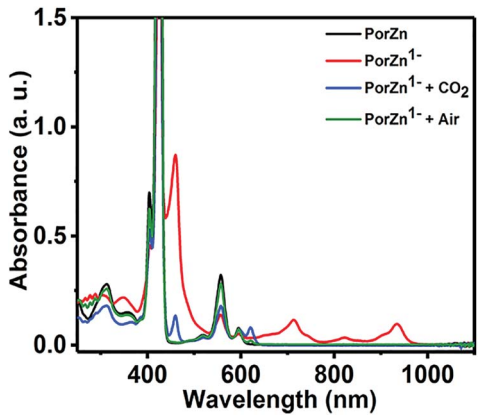


Fig. 5 Absorption spectra of ZnTPP (black line), its reduced species (red line) produced by the reduction of ZnTPP by sodium naphthalenide, and the reduced species after exposure to $CO_2$ (blue line) or air (green line) in THF. Reprinted with permission from ref. 95. Copyright 2017, American Chemical Society.

million TON at an applied potential of −2.8 V in a DMF solution containing [$^n$Bu$_4$N][PF$_6$] (0.1 M) and trifluoroethanol (1.2 M) under a $CO_2$ atmosphere.[96] When the pendant N–H group was replaced by a N–Me group, TONs became 300 times lower than that of **I**, indicating that the presence of the pendant NH moiety of the secondary amine is crucial for catalysis.[96,97] Moreover, the presence of NH groups leads to a positive shift in the reduction potential of the $Co^{I/0}$ couple, resulting in a decrease in the overpotential for $CO_2$ reduction. Complex **I** is reduced by one electron to generate the $Co^I$ complex, which is further reduced to the $Co^0$ form. $CO_2$ binds to the $Co^0$ complex to produce the

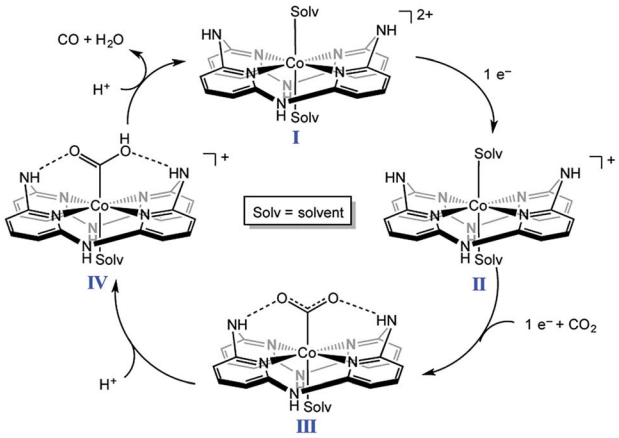


Scheme 5 Catalytic cycle of two-electron reduction of $CO_2$ to CO with a nonheme cobalt complex with a macrocyclic aminopyridine (I). Reprinted with permission from ref. 96. Copyright 2016, American Chemical Society.

$CO_2$ adduct ([Co(CO$_2$)]$^0$, **III** in Scheme 5), which is stabilised by intramolecular H-bonds of the pendant secondary amines.[96] The successive protonation of the $CO_2$ complex affords CO and $H_2O$ to regeneratecomplex **I**.[96,97]

The [Co$^{II}$(qpy)(H$_2$O)$_2$]$^{2+}$ (qpy = 2,2′:6′,2″:6″,2‴-quaterpyridine) complex also efficiently catalyses the electrochemical $CO_2$-to-CO conversion in an MeCN solution in the presence of weak Brønsted acids.[98] Controlled potential electrolysis (CPE) was performed at −1.1 V *vs.* SCE in the presence of 3 M PhOH, corresponding to 140 mV overpotential. CO was produced with 96% catalytic selectivity (a small amount of $H_2$ (4%) was obtained as the only byproduct) and 94% faradaic efficiency.[98] The [Co$^{II}$(qpy)(H$_2$O)$_2$]$^{2+}$ complex is an excellent catalyst, at a very low overpotential, better than active Mn complexes (*vide infra*),[99–103] being only surpassed by the Fe tetraphenylporphyrin bearing four trimethylammonium groups in the *ortho* position of each phenyl (complex a in Fig. 6).[88]

Rhenium bipyridine complexes (Re(bpy)(CO)$_3$Cl and its derivatives)[104–108] and manganese complexes (Mn(bpy)(CO)$_3$Br and its derivatives)[109–114] are known to act as catalysts for electrocatalytic reduction of $CO_2$ to CO. The catalytic mechanisms have been investigated extensively using various spectroscopic methods including UV/Vis absorption and pulsed-EPR techniques (2P-ESEEM and HYSCORE) combined with DFT calculations.[113] A key intermediate in the catalytic cycle of $CO_2$ reduction is demonstrated to be a low spin Mn$^{II}$–hydroxycarbonyl complex after the oxidative addition of $CO_2$ and $H^+$ to a $Mn^0$ carbonyl dimer (Scheme 6).[113]

The catalytic activity of a manganese complex *fac*-[MnBr(4,4′-bis(phosphonic acid)-2,2′-bipyridine)(CO)$_3$] (**MnP**) for CO production was improved when immobilized on a mesoporous $TiO_2$ electrode ($TiO_2$/**MnP**).[114] Controlled potential electrolysis of $TiO_2$/**MnP** at $E_{appl} = -1.7$ V *vs.* $Fc^+$/Fc ($\eta = 0.42$ V) under $CO_2$ in MeCN/$H_2O$ (19/1) for 2 h passed an average charge of 1.10 ± 0.25 Coulombs with a faradaic efficiency of 67 ± 5% and a TON of 112 ± 17 for CO. The faradaic yield of $H_2$ for this system was 12.4 ± 1.4% and formate was not detected by ion chromatography.[114]

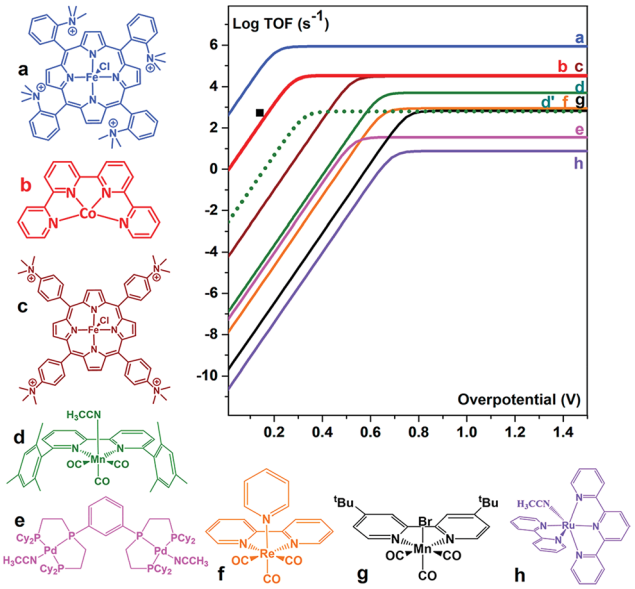


Fig. 6 Comparison of the metal catalysts (a,[88] b,[98] c,[88] d,[99] e,[100] f,[101] g,[102] and h[103]) for the $CO_2$-to-CO electrochemical conversion in DMF or MeCN by means of their catalytic Tafel plots (log TOF as a function of the overpotential ($\eta = E^0(CO_2/CO) - E$). d′ dotted lines: data for complex d in the presence of 0.1 M $Mg^{2+}$.[99] ■: TOF value for b. Reprinted with permission from ref. 98. Copyright 2018, American Chemical Society.

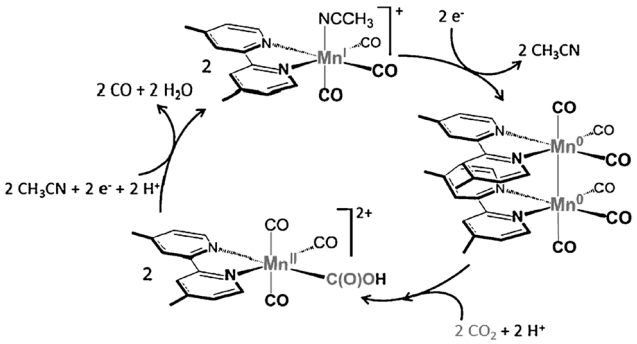


Scheme 6 The catalytic cycle for two-electron reduction of $CO_2$ to CO with $[Mn(bpy)(CO)_3]^+$. Reprinted with permission from ref. 113. Copyright 2014, WILEY-VCH Verlag GmbH.

The high activity and low overpotential of $TiO_2$/**MnP** are suggested to result from temporary desorption of the catalyst, followed by dimerization and re-anchoring within mesoporous $TiO_2$, because phosphonic acid modified molecules, such as **MnP**, display some lability when bound to $TiO_2$.[115] The high local concentration of **MnP** may also place the metal centres in an environment where they are predisposed to dimerization upon reduction.[114]

The lowest overpotential for the electrocatalytic reduction of $CO_2$ to CO was achieved by using a manganese complex, [Mn{4,4′-di(1*H*-pyrrolyl-3-propyl carbonate)-2,2′-bipyridine}$(CO)_3$-MeCN]$^+(PF_6)^-$ loaded onto conductive MWCNTs ([Mn-MeCN]/MWCNT), which exhibited catalysis at −0.21 V *vs.* SHE (overpotential of about 100 mV for CO production).[116] The MWCNTs together with surface adsorbed $K^+$ ions provided an environment to stabilize $CO_2$ adjacent to the Mn complex and significantly lowered the overpotential for $CO_2$ reduction in an aqueous solution.[116]

A case of selectivity tuning was observed as a function of ligand type when Ni(II) complexes in Fig. 7 were employed as catalysts for $CO_2$ reduction.[117] Controlled potential electrolyses were carried out with each member of the catalyst series (Fig. 7) in $CO_2$-saturated MeCN solutions containing 2% $H_2O$.[117] The 15-membered macrocyclic complex (**3-Ni**) gave high selectivity for $CO_2$ reduction to CO with a faradaic efficiency of 87%, the remaining 11% faradaic yield resulted in $H_2$ generation at an applied potential of 2.44 V *vs.* $Fc^+/Fc$.[116] On the other hand, **1-Ni** supported by a non-macrocyclic ligand gave a faradaic efficiency of 93% for $H_2$ and only 5% for CO, whereas the less rigid 16-membered macrocyclic complex (**2-Ni**) exhibited moderate selectivity for both CO (56%) and $H_2$ (43%) evolution in the presence of $CO_2$ and $H_2O$.[117] Thus, increased rigidity of the redox-active macrocycle leads to enhanced selectivity for $CO_2$ reduction to CO over the competing hydrogen evolution reaction.[117]

The first electron reduction of **1-Ni** is calculated to be that of the metal center and the second electron reduction is calculated to be ligand-based to produce the $[Ni^I(L^\bullet)]$ species. The $[Ni^I(L^\bullet)]$ complex reacts with $H^+$ to form a metal hydride, from which $H_2$ is produced through a reaction with another $H^+$.[117] In contrast, the first and second reductions of **3-Ni** are calculated to be both ligand-centered, and the resulting $[Ni^{II}(L^{2\bullet})]$ complex is not capable of metal hydride generation, and therefore leads to no $H_2$ production. The two-electron reduced species of **2-Ni** is best described by resonance forms $[Ni^{II}(L^{2\bullet})] \leftrightarrow [Ni^I(L^\bullet)]$, which are capable of producing both CO and $H_2$.[117]

A nickel complex supported by a pincer-type carbene–pyridine–carbene ligand also exhibited high selectivity for the electrocatalytic reduction of $CO_2$ to CO over proton reduction.[118] A series of $Ni^{II}$ macrocycle complexes structurally similar to $[Ni(cyclam)]^{2+}$ (cyclam = 1,4,8,11-tetraazacyclotetradecane) also act as selective electrocatalysts for CO production over $H_2$ at a mercury pool working electrode in an aqueous solution.[119–121] At pH 5, with an applied potential of −0.96 V *vs.* NHE (overpotential of −0.55 V), the Ni complexes are efficient, having high faradaic efficiencies for the selective reduction of $CO_2$ to CO.[118] Hg provides favorable noncovalent dispersive interactions with the cyclam ligand to destabilise the poisoned CO-bound form of the catalyst, leading to enhanced catalytic reactivity.[122] The binding of $CO_2$ to Ni(I) complexes has been

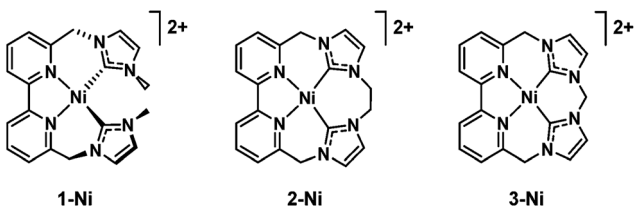


Fig. 7 Nickel(II) catalysts supported by non-macrocyclic and macrocyclic bipyridyl-NHC ligands. Reprinted with permission from ref. 117. Copyright 2018, Royal Society of Chemistry.

extensively studied by pulse radiolysis measurements to demonstrate that the formation of the Ni(I)–$CO_2$ adduct is in equilibrium between the Ni(I) complex and free $CO_2$.[123,124]

## 5 Electrocatalytic reduction of $CO_2$ to HCOOH with heme and nonheme metal complexes

The two-electron/two-proton reduction of $CO_2$ also affords formate ($HCOO^-$) as well as CO.[125] The reduced metal complex ($M^-$) may react directly with $CO_2$ to produce the M–$CO_2^-$ adduct that is further reduced with $H^+$ to evolve CO and $H_2O$ (Scheme 7) as in the case of the iron porphyrin in Scheme 3.[125] Alternatively $M^-$ can react with $H^+$ to generate the hydride complex (MH) capable of direct reaction with a proton to produce $H_2$, or alternatively couple with $CO_2$ to produce $HCOO^-$ (Scheme 7).[125] Whether the catalytic two-electron/two-proton reduction of $CO_2$ affords CO or $HCOO^-$ depends on the interplay of metals and ligands of the implemented catalyst.[126]

A series of metalloprotoporphyrins (MPPs in Fig. 8) were employed as catalysts for the electrochemical reduction of $CO_2$ in an aqueous solution. Formic acid was not obtained when CrPP, MnPP, CoPP and FePP were used as catalysts. In the case of CoPP, CO was produced selectively at pH 3 with high faradaic efficiency.[126] Exercising the reaction with InPP, CrPP, SnPP and GaPP as catalysts, no gaseous products other than $H_2$ were observed. When SnPP, InPP and RhPP were employed as catalysts, however, significant amounts of formic acid were produced depending on the pH as shown in Fig. 9, where the faradaic efficiency of $HCOO^-$ with InPP at pH 9.6 was optimal, reaching a value close to 70%.[126] At very low pHs, hydrogen evolution dominated, resulting in little or no HCOOH production.[126] At very alkaline pHs, the $H_2$ production also seemed to be dominant, leading to poor selectivity towards $HCOO^-$.[126] The catalytic mechanisms for $HCOO^-$ production with InPP, SnPP and RhPP have not yet been clarified.

In contrast to iron porphyrins that catalyse the two-electron reduction of $CO_2$ to CO (Scheme 1), a nonheme iron(III) chloride complex bearing a 6,6′-di(3,5-di-*tert*-butyl-2-hydroxybenzene)-2,2′-bipyridine ($^{tbu}$dhbpy) ligand, Fe($^{tbu}$dhbpy)Cl, catalyses the electrochemical two-electron reduction of $CO_2$ to formate in the presence of phenol (0.50 M) as a proton source in DMF with a faradaic efficiency of 68 ± 4% together with $H_2$ as a minor product (30 ± 10% faradaic efficiency) and minimal CO (1.1 ± 0.3% faradaic efficiency) at −2.5 V *vs.* $Fc/Fc^+$.[127] The first one-electron reduction of Fe($^{tbu}$dhbpy)Cl ($Fe^{III/II}$; $E^0 = -0.89$ V *vs.* $Fc/Fc^+$) exhibited a Nernstian PhOH-dependent electrochemical response, which suggests that the reduction is coupled with protonation of a bound phenolate moiety of the ligand framework by a PhOH proton donor as shown in Scheme 8.[127] At the second reduction potential ($E^0 = -2.09$ V *vs.* $Fc/Fc^+$), a second protonation event occurs at the metal centre to produce the iron(III)–hydride complex. At the third reduction potential ($E^0 = -2.65$ V *vs.* $Fc/Fc^+$), the catalytic activity was observed in the presence of PhOH as a sacrificial proton donor when the Fe(II)–hydride complex reacts with $CO_2$ to produce the formate complex from which formate is released to regenerate the Fe(II) complex (Scheme 8).[127] A kinetic isotope effect (KIE) of 4.8 ± 0.9 was observed when PhOD is used instead of PhOH, indicating that the insertion of $CO_2$ into the Fe(II)–hydride complex is the rate-determining step.[127] Fe(II)–hydride complexes were reported to hydrogenate $CO_2$ to produce formate.[128–130] An iron cluster hydride $[HFe_4N(CO)_{12}]^-$ is also reported as an effective catalyst for the electrochemical reduction of $CO_2$ to formate under mild conditions of pH 7 buffered aqueous solution and an applied potential of −1.2 V *vs.* SCE.[131,132]

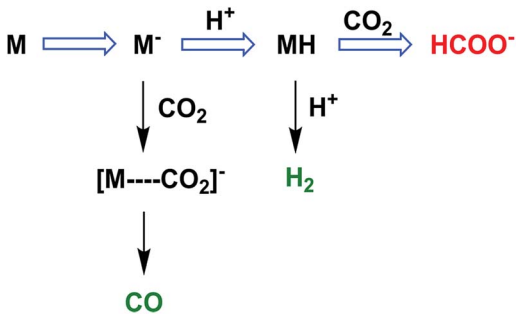


Scheme 7 The reaction pathway of two-electron reduction of $CO_2$ with a metal complex (M) to produce $HCOO^-$ or CO. Reprinted with permission from ref. 125. Copyright 2017, American Chemical Society.

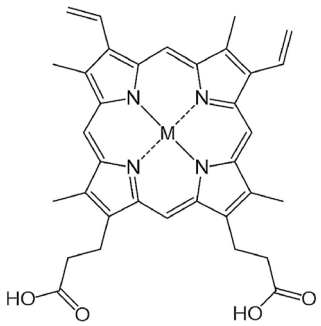


Fig. 8 Chemical structure of metalloprotoporphyrins (MPP). Reprinted with permission from ref. 126. Copyright 2017, Elsevier.

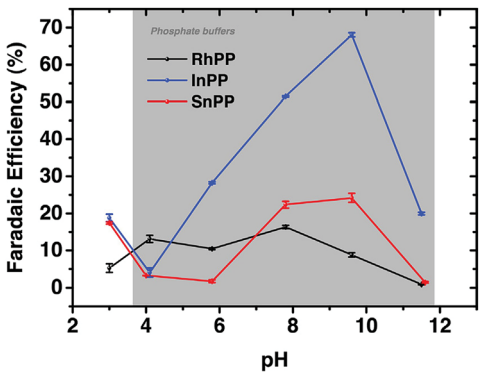


Fig. 9 Faradaic efficiencies for the electrocatalytic reduction of $CO_2$ to HCOOH or $HCOO^-$ with RhPP, InPP and SnPP, determined at $t$ = 10 min, at $E = -1.5$ V *vs.* RHE as function of pH. Reprinted with permission from ref. 126. Copyright 2017, Elsevier.

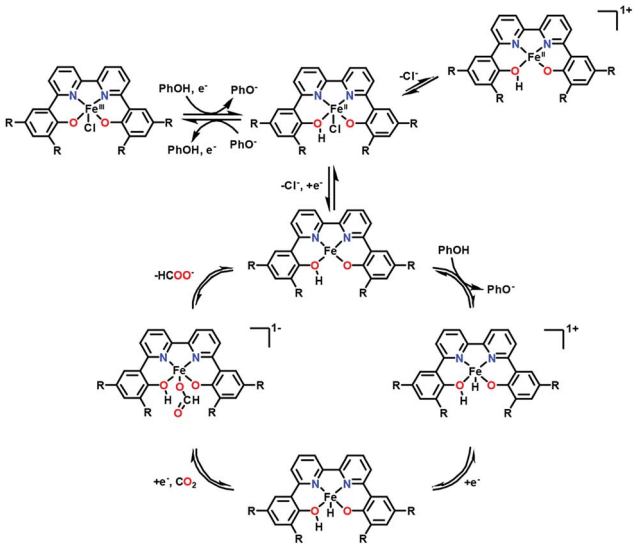


Scheme 8 Catalytic cycle for two-electron reduction of $CO_2$ to CO with a nonheme iron(III) chloride complex bearing a 6,6′-di(3,5-di-*tert*-butyl-2-hydroxybenzene)-2,2′-bipyridine ligand (Fe($^{tbu}$dhbpy)Cl) *via* protonation by phenol. Reprinted with permission from ref. 127. Copyright 2018, American Chemical Society.

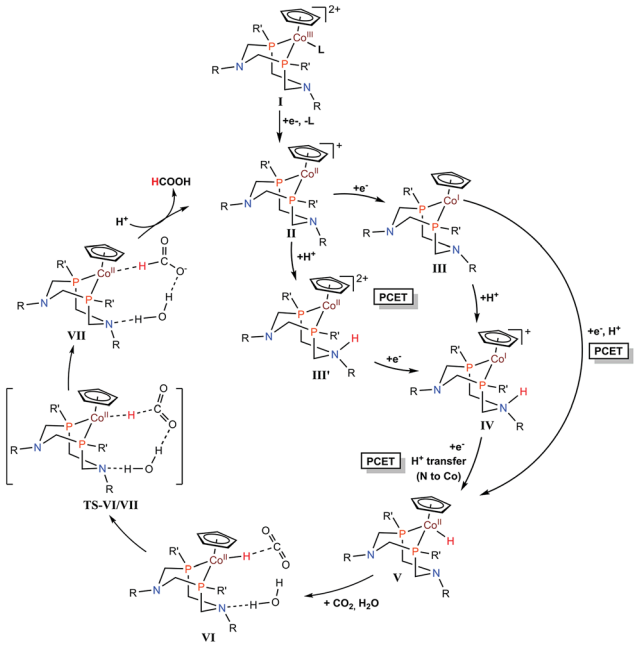


Scheme 9 Catalytic cycle for two-electron reduction of $CO_2$ to CO with $[CpCo(P^R_2N^{R'}_2)I]^+$ complexes containing diphosphine ligands ($P^R_2N^{R'}_2$) with two pendant amine residues. Reprinted with permission from ref. 133. Copyright 2017, American Chemical Society.

Cobalt complexes ($[CpCo(P^R_2N^{R'}_2)I]^+$) containing diphosphine ligands ($P^R_2N^{R'}_2$) with two pendant amine residues catalyse the production of formic acid in DMF/water mixtures with a faradaic efficiency of 90 ± 10% at 500–700 mV overpotentials.[133] The $[CpCo(P^R_2N^{R'}_2)I]^+$ complex with R = cyclohexyl and R′ = benzyl exhibited the best catalytic activity with a TON for HCOOH of 23 and 15 in the presence of 1.1 and 0.56 M water, respectively, after electrolyses at −2.25 V *vs.* $Fc/Fc^+$ for 1 h.[133] The electrocatalytic mechanism for $CO_2$ reduction to formate is proposed as shown in Scheme 9, where a $Co^{II}$–hydride intermediate hydrogenates $CO_2$ to produce formate. After two successive electron transfers, a $Co^I$ species (complex III in Scheme 9) is generated. This species is then protonated and further reduced to form a cobalt(II)–hydride ($Co^{II}$–H) complex (complex V in Scheme 9).[133] DFT calculations indicated that the protonation of the pendant amine in either the $Co^{II}$ or $Co^I$ states allows two other pathways *via* intermediates III′ and IV, respectively, through intramolecular proton transfer to the cobalt centre with the reduction of the metal center.[133] The $Co^{II}$–H species V then reacts with $CO_2$, generating complex VI. Internal hydride transfer from cobalt to $CO_2$ then yields complex VII.[133] The release of formic acid from complex VII regenerates the $Co^{II}$ species (complex II in Scheme 9) and completes the catalytic cycle.[133]

The product selectivity of electrocatalytic reduction of $CO_2$ to CO *vs.* HCOOH with the assembly of a [MnBr(2,2′-bipyridine)$(CO)_3$] complex anchored to a carbon nanotube electrode *via* a pyrene unit was examined, and reported to be tuned by variation of metal complex density on the nanotube surface, where CO was observed as the main product at high catalyst loadings, and formate was the dominant $CO_2$ reduction product at low catalyst loadings.[134] The formation of a dimeric $Mn^0$ species at higher surface loading preferentially leads to CO formation, whereas at lower surface loading the electrochemical generation of a monomeric Mn–hydride is suggested to enhance the production of formate (Scheme 10).[134] The Mn–CNT hybrid catalyst exhibited much higher activity for electrocatalytic reduction of aqueous $CO_2$ with TONs of up to 1790 ± 290 for CO ($\eta$ = 550 mV) and up to 3920 ± 230 for formate ($\eta$ = 590 mV),[134] compared to electrolyses in the absence of carbon nanotubes.[135–137]

When a Ni(bis-dithiolene) complex with a quinoxaline-pyran-fused dithiolene ligand ($qpdt^{2-}$) (see the X-ray crystal structure in Fig. 10) was employed as a $CO_2$ reduction catalyst using a Hg/Au amalgam electrode, formate as the major product together with minor amounts of CO and $H_2$ was observed at reasonable overpotentials with good faradaic yield and notable stability.[138] The onset potential of the catalytic wave with

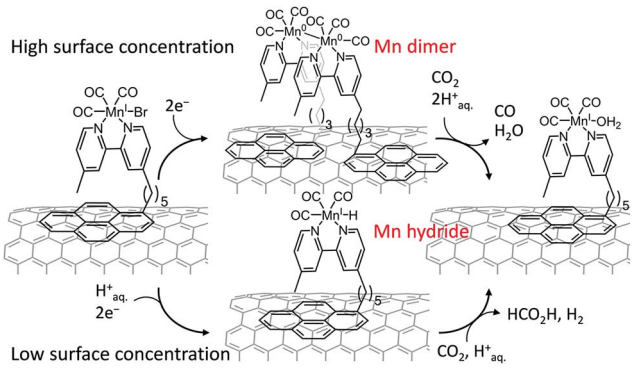


Scheme 10 Two-electron reduction of $CO_2$ to CO *vs.* HCOOH with the [MnBr(2,2′-bipyridine)$(CO)_3$] complex anchored to a carbon nanotube electrode *via* a pyrene unit depending on the surface concentration. Reprinted with permission from ref. 134. Copyright 2017, American Chemical Society.

$[Ni(qpdt)_2]^-$ was observed at approximately −1.7 V *vs.* Ag/AgCl (=−1.5 V *vs.* SHE), with a halfwave potential at −1.80 V and a peak at −2 V.[138] The overpotential was determined to be ~340 mV by comparing the experimental onset potential to the standard potential of the $CO_2$/HCOOH couple in MeCN in the presence of trifluoroethanol as a proton source.[138] During the electrolysis, a complete reduction of the ligand occurred, followed by the subsequent pyran ring opening to produce the real catalyst ($[Ni^{II}(L)_2]^{2-}$; L is a pyran ring-opened ligand produced from $qpdt^{2-}$ by electrolysis) as shown in Scheme 11.[138] A Ni–hydride intermediate $[Ni^{III}(H)(L)_2]^{2-}$ was proposed to be a catalytically relevant species for $CO_2$ reduction to formate, which was produced by one-electron reduction of $[Ni^{II}(L)_2]^{2-}$, followed by the reaction of $[Ni^{I}(L)_2]^{3-}$ with $H^+$.[138] The $[Ni^{III}(H)(L)_2]^{2-}$ species reacts with $CO_2$, followed by a release of $HCOO^-$ and regeneration of $[Ni^{II}(L)_2]^{2-}$ upon the one-electron reduction at −0.51 V *vs.* Ag/AgCl.[138]

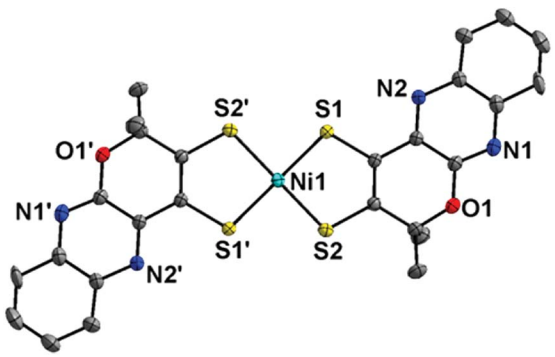


Fig. 10 X-ray crystal structure of a $Ni^{III}$(bis-dithiolene) complex with a quinoxaline-pyran-fused dithiolene dianion ligand ($qpdt^{2-}$) ($[Ni^{III}(qpdt)_2]^-$) at 50% probability. Hydrogen atoms are omitted for clarity. Reprinted with permission from ref. 138. Copyright 2018, American Chemical Society.

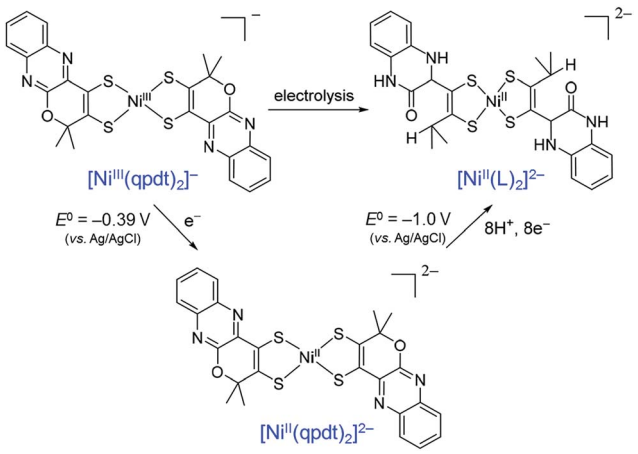


Scheme 11 Electrochemical reduction of $[Ni(qpdt)_2]^-$, followed by the subsequent pyran ring opening to produce the real catalyst ($[Ni^{II}(L)_2]^{2-}$; L is a pyran ring-opened ligand produced from $qpdt^{2-}$ by electrolysis) during electrolysis. Reprinted with permission from ref. 138. Copyright 2018, American Chemical Society.

A small amount of CO observed during the electrolysis was proposed to be produced *via* the $\eta^1$-$CO_2$ species based on the DFT calculations.[138] Although many $\eta^2$-$CO_2$ nickel structures have been known to date,[139–143] a rare $\eta^1$-$\kappa$C binding mode of $CO_2$ to Ni was also reported by utilizing an anionic tridentate PNP ligand ($PNP^- = N[2\text{-}P^iPr_2\text{-}4\text{-}Me\text{-}C_6H_3]_2^-$).[144,145] The protonation of the $\eta^1$-$CO_2$ species affords the carboxylate intermediate ($[Ni(C(O)OH)(L)_2]^{2-}$), which undergoes a heterolytic C–O bond cleavage to generate $[Ni(CO)(L)_2]^-$ upon protonation, followed by the release of CO.[138,146]

## 6 Further electrocatalytic reduction of CO to fuels with metalloporphyrins

The electrochemical reduction of $CO_2$ to CO and its further reduction to methane were made possible by using a simple Co protoporphyrin molecular catalyst immobilized onto a pyrolytic graphite (PG) electrode (CoPP-PG).[147] In an aqueous solution with a pH value of 1, the faradaic efficiency for methane production is larger than that for CO, but the dominant product is $H_2$.[147] At pH = 3, CO became a major product, especially at less cathodic potentials, where the faradaic efficiency for CO was 40%.[147] The efficiency towards CO can be further increased by performing the experiment at higher $CO_2$ pressure (10 atm), which leads to a faradaic efficiency of 60% at a potential of −0.6 V (Fig. 11).[147]

The mechanism of catalytic $CO_2$ reduction to CO by CoPP may be similar to that of iron porphyrins in Scheme 1. The reduction of $Co^{II}PP$ to $[Co^{I}PP]^-$ is coupled with $CO_2$ binding to afford the $CO_2$ adduct that reacts with water to produce the $Co^{III}PP$–C(O)OH adduct, which is further reduced to produce the $Co^{II}PP$–CO adduct as shown in Scheme 12.[147] The two-electron/two-proton reduction of the $Co^{II}PP$–CO adduct affords the $Co^{II}PP$–HCHO adduct that is further reduced by four electrons with four protons to finally yield methane and water, accompanied by the regeneration of $Co^{II}PP$ (Scheme 12).[147] The formation of CO is more favoured than $H_2$ at higher pHs.[147] However, further reduction of CO is more favoured at a low pH.[147] Thus, the faradaic yield of methane was higher than that of CO at pH 1, while $H_2$ remained the major product.[147]

Crystallized copper phthalocyanine supported on carbon black (CuPc/CB) was reported to exhibit high selectivity for $C_2H_4$ with a maximum faradaic efficiency of 25% under atmospheric pressure at −1.6 V *vs.* Ag/AgCl (=−1.4 V *vs.* SHE), while $CH_4$ and CO were also generated as minor products (Fig. 12).[148] In contrast to the crystalline form of CuPc/CB, the noncrystalline CuPc/CB catalyst showed a much lower selectivity and reactivity for $C_2H_4$ production.[148] When noncrystalline CuPc was treated with Milli-Q water and chloroform to completely restore its crystallinity, the restored crystalline CuPc/CB catalyst afforded faradaic efficiency and partial current density values as high as those of the original crystalline CuPc/CB catalyst.[148] These results indicate that catalyst crystallinity is crucial for the selective conversion of $CO_2$ to $C_2H_4$, because the C–C bond forming step to produce $C_2H_4$ from CO is likely mediated by two metal centers.[148]

 

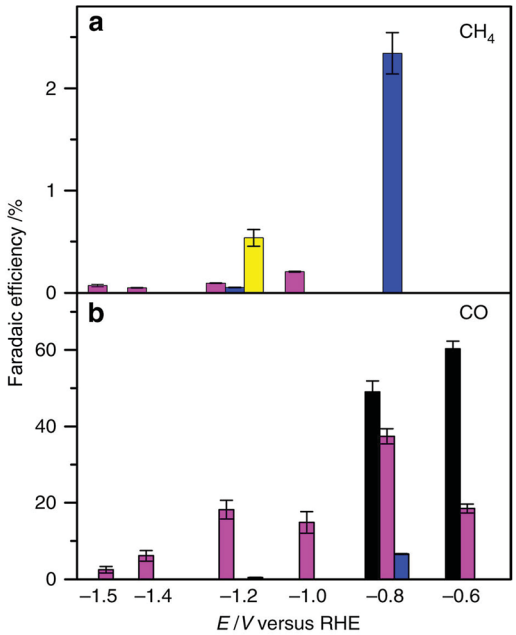


Fig. 11 Faradaic efficiency (FE) for the electrocatalytic $CO_2$ reduction to (a) $CH_4$ and (b) CO in 0.1 M perchlorate solution saturated with $CO_2$ conducted at each applied potential for 1 h and 90 min at $P_{CO_2} = 1$ atm and 10 atm, respectively [yellow bars: pH = 1, $P_{CO_2} = 1$ atm; blue bars: pH = 1, $P_{CO_2} = 10$ atm; magenta bars: pH = 3, $P_{CO_2} = 1$ atm and black bars pH = 3, $P_{CO_2} = 10$ atm]. Reprinted with permission from ref. 147. Copyright 2015, Nature Publishing Group.

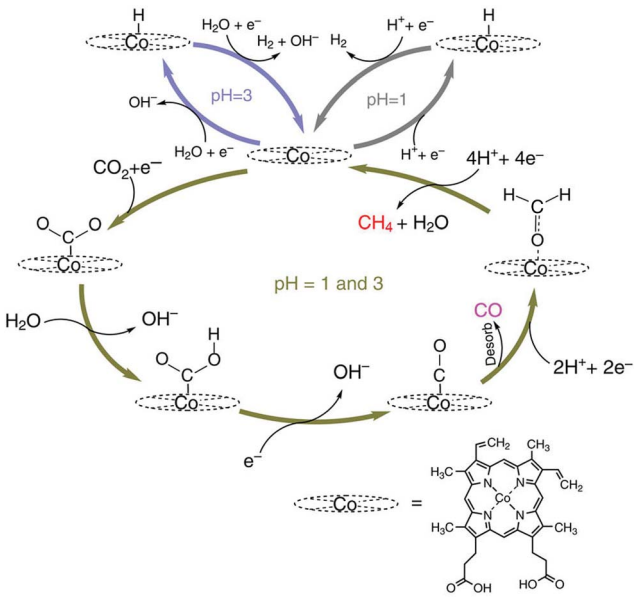


Scheme 12 Catalytic cycle for two electron reduction of $CO_2$ to CO and further reduction to $CH_4$ with a Co protoporphyrin molecular catalyst (CoPP) immobilized onto a pyrolytic graphite (PG) electrode (CoPP-PG). Reprinted with permission from ref. 147. Copyright 2015, Nature Publishing Group.

Heterobimetallic cavities formed by the face-to-face coordination of thiol-terminated iron porphyrins on copper electrodes *via* self-assembly of supramolecular cages (M = Fe in Fig. 13)

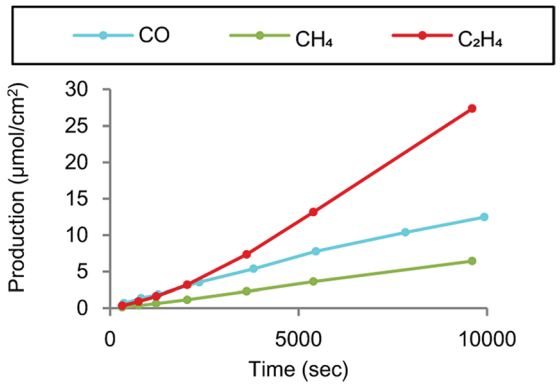


Fig. 12 Products derived from $CO_2$ electrochemical reduction by crystalline CuPc/C at −1.6 V *vs.* Ag/AgCl in a two-compartment H-cell. Reprinted with permission from ref. 148. Copyright 2017, American Chemical Society.

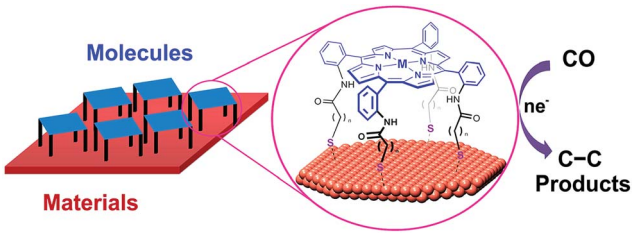


Fig. 13 Schematic illustration of supramolecular assembly of cages between molecular components and supramolecular assembly of cages between molecular components and a copper electrode. Reprinted with permission from ref. 149. Copyright 2017, American Chemical Society.

have made it possible to convert CO to $C_2$ products *via* C–C bond formation in aqueous electrochemical CO reduction with high faradaic efficiency (83% total with 57% to ethanol) and current density (1.34 mA $cm^{-2}$) at a potential of −0.40 V *vs.* RHE.[149] The cage-functionalized electrodes afforded an order of magnitude improvement in both selectivity and activity for electrocatalytic CO reduction compared to their parent copper surfaces.[149] Control analogues that lack thiol binding groups as well as positional isomers favouring edge-on binding or direct van der Waals stacking exhibited reduced surface access and negligible CO over water reduction selectivity, suggesting the critical role of the three-dimensional pockets in catalysis, where the Fe centre can aid in the cooperative reduction of potential acetaldehyde intermediates.[149]

## 7 Photocatalytic reduction of $CO_2$ with heme and nonheme metal complexes

The electrocatalytic reduction of $CO_2$ can be replaced by photocatalytic reduction using photocatalysts instead of electrocatalysts. For example, the selective electrocatalytic reduction of $CO_2$ to CO with a glassy carbon electrode modified with a cobalt(II) chlorin complex ($Co^{II}$(Ch)) adsorbed on MWCNTs

($Co^{II}$(Ch)/MWCNTs; see Fig. 3 for the schematic image) is replaced by the photocatalytic reduction of $CO_2$ with trimethylamine (TEA) using $Co^{II}$(Ch)/MWCNTs as a $CO_2$ reduction catalyst and $[Ru^{II}(Me_2phen)_3]^{2+}$ ($Me_2phen$ = 4,7-dimethyl-1,10-phenanthroline) as a sensitizer.[150] The photocatalytic mechanism of the $CO_2$ reduction is shown in Scheme 13, where electron transfer from TEA to the excited state of $[Ru^{II}(Me_2phen)_3]^{2+}$ ($[Ru^{II}(Me_2phen)_3]^{2+}$*: * denotes the excited state) occurs to produce TEA radical cations and $[Ru^{I}(Me_2phen)_3]^{+}$ that reduces $Co^{II}$(Ch) to $[Co^{I}(Ch)]^{-}$.[150] $[Co^{I}(Ch)]^{-}$ reacts with $CO_2$ to produce the $[(Ch)Co^{III}(CO_2)]^{-}$ complex that is protonated to produce $Co^{II}$(Ch)COOH, from which water is released by the protonation to produce the $[Co^{III}(Ch)CO]^{+}$ complex.[150] After the CO release from the Co(III)CO complex, the Co(III) complex is reduced by TEA to regenerate $Co^{II}$(Ch). Hydrogen evolution simultaneously occurs as a side reaction, much like in the electrocatalytic case, because $[Co^{I}(Ch)]^{-}$ can also react with $H^+$ to produce the hydride complex ($[Co^{III}(Ch)(H)]$), which then can couple to a $H^+$ to produce $H_2$.[151] The TON of the photocatalytic reduction was determined to be 710 with the ratio of CO to $H_2$ of 2.4 : 1 in 20 h when 5.0 μM of $Co^{II}$(Ch) and 1.0 mg of MWCNTs were used.[150] The π–π interaction between MWCNTs and $Co^{II}$(Ch) may provide a suitable hydrophobic environment for the selective binding of $CO_2$ over protons, because the binding of $CO_2$ to the Co(I) complex is required for the formation of CO (Scheme 13).[150]

An iron tetraphenylporphyrin complex functionalized with trimethylanilinium groups (Fe-*p*-TMA in Fig. 2), which is an efficient and selective molecular electrocatalyst for converting $CO_2$ to CO,[88] can also act as an efficient catalyst in photocatalytic reduction of $CO_2$ to methane using Ir(ppy) (ppy = phenylpyridine) as a dye under visible light irradiation at ambient temperature and pressure.[152,153] The catalytic system, which was evaluated in an acetonitrile solution containing a photosensitizer (Ir(ppy)), sacrificial electron donor (TEA) and proton source (trifluoroethanol), operates stably under irradiation over several days to produce CO, $CH_4$, and $H_2$ with turnover numbers (and selectivities) of 367 (78%), 79 (17%) and 26 (5%), respectively in 107 h.[152] These values correspond to a methane production rate of 763 μmol per hour per gram of catalyst (μmol $h^{-1}$ $g^{-1}$), which is larger than those obtained using other catalysts[154–159] that generate methane from $CO_2$. Trifluoroethanol facilitates the C–O bond cleavage step as observed in the electrocatalytic reduction of $CO_2$ (Scheme 3).[84] No other gaseous product, methanol, formaldehyde or formate was produced.[152] Isotopic labelling experiments conducted under a $^{12}CO_2$ or a $^{13}CO_2$ atmosphere confirmed that methane was produced from $CO_2$. A two-step procedure, that first reduces $CO_2$ to CO and then reduces CO to further reduced species of CO, generates methane with a selectivity of up to 82% and a quantum yield (light-to-product efficiency) of 0.18%.[152]

The photocatalytic mechanism for $CO_2$ reduction to methane is proposed as shown in Scheme 14, where the starting $Fe^{III}$ porphyrin is reduced with three electrons by Ir(ppy)* to the catalytically active $Fe^0$ species.[152] The $Fe^0$ species reduces $CO_2$ to CO through a two-step protonation of the $Fe^0$ species by $CF_3$-$CH_2OH$ with dehydration (right-hand iron cycle) as in the case of the electrocatalytic reduction of $CO_2$ to CO in Scheme 3, where AH = trifluoroethanol.[84] The CO produced binds to $Fe^{II}$ and is further reduced by a total of six electrons by electron transfer from Ir(ppy)* and six protons to generate $CH_4$ (and $H_2O$), through a postulated $Fe^{I}$-formyl ($Fe^{I}CHO$) intermediate (left-hand iron cycle).[152]

Not all photocatalytic systems employ separately a catalyst and a photosensitizer. Fe-*p*-TMA can also catalyse the photocatalytic reduction of $CO_2$ to CO with 1,3-dimethyl-2-phenyl-2,3-dihydro-1*H*-benzo[*d*]-imidazole (BIH) selectively under visible light irradiation without the assistance of an additional photosensitizer.[160] BIH was reported to enhance the photocatalytic formation of CO from $CO_2$,[161,162] due to its high reductive ability ($E_{ox}$ = +0.33 V *vs.* SCE = +0.57 *vs.* SHE),[163] its fast deprotonation to $BI^{\bullet}$ once oxidized and its overall two-electron donation capacity ($BI^{\bullet}$ could be in turn easily oxidized to $BI^{+}$).

BIH was also used as a sacrificial reductant together with triethanolamine (TEOA) for visible-light driven $CO_2$ reduction in MeCN using $[Ru(bpy)_3]^{2+}$ (bpy = 2,2′-bipyridine) as a photosensitizer and a $Cu^{II}$ complex bearing 2,2′:6′,2″:6″,2‴-quaterpyridine (qpy) ($[Cu(qpy)]^{2+}$) as a selective reduction catalyst.[164] The photocatalytic reaction is greatly enhanced by the presence of $H_2O$ (1–4% v/v), and a TON of >12 400 for CO

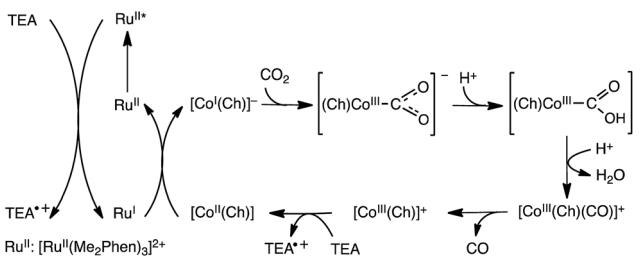


Scheme 13 Photocatalytic cycle for two-electron reduction of $CO_2$ to CO with a cobalt(II) chlorin complex ($Co^{II}$(Ch)) adsorbed on multi-walled carbon nanotubes ($Co^{II}$(Ch)/MWCNTs). Reprinted with permission from ref. 150. Copyright 2016, Royal Society of Chemistry.

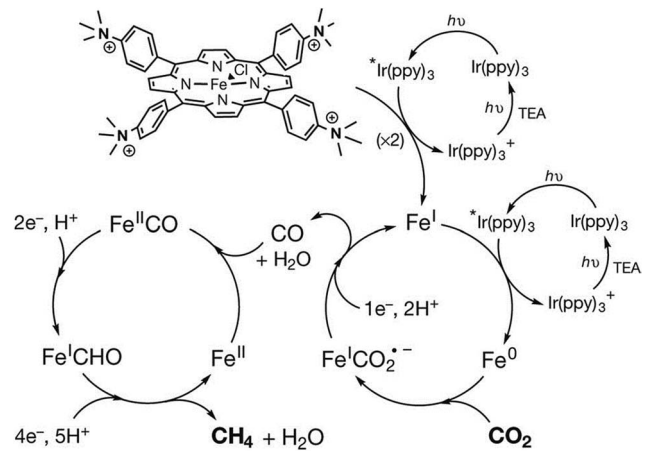


Scheme 14 Photocatalytic cycles for two-electron reduction of $CO_2$ to CO and further reduction to $CH_4$ with Fe-*p*-TMA and $Ir(ppy)_3$. Reprinted with permission from ref. 152. Copyright 2017, Macmillan Publishers Limited, part of Springer Nature.

production has been achieved with 97% selectivity, which is among the highest of molecular 3d-metal $CO_2$ reduction catalysts.[164] It was confirmed that the photocatalyst remains homogeneous based on results from Hg poisoning and dynamic light scattering experiments.[164]

BIH alone acts as an electron donor in the photocatalytic reduction of $CO_2$ to CO with a Ni(II) complex bearing an $S_2N_2$-type tetradentate ligand, $[Ni^{II}(bpet)]^{2+}$ (bpet = bis(2-pyridylmethyl)-1,2-ethanedithiol), as a $CO_2$ reduction catalyst and $[Ru(bpy)_3]^{2+}$ as a photosensitizer in a DMA/$H_2O$ solution mixture (9 : 1 v/v) under a $CO_2$ atmosphere at 298 K.[165] In this photocatalytic system, the $[Ni^{II}(bpet)]^{2+}$ complex showed a high TON exceeding 700 with a very high CO selectivity of >99% and a quantum yield of 1.42%.[165]

Composite electrodes formed by a combination of an organic-semiconductor with a metal-porphyrinoid catalyst were also evaluated as photocatalysts for $CO_2$ reduction. Graphite carbon nitride (g-$C_3N_4$), which has frequently been used as an organic semiconductor photocatalyst,[166–169] was modified with a carboxyl group of tetra(4-carboxyphenyl)porphyrin iron(III) chloride (FeTCPP) to prepare a g-$C_3N_4$ nanosheets/FeTCPP (g-$C_3N_4$/FeTCPP) heterogeneous catalyst. The material was then implemented for the photoreduction of $CO_2$ to CO with TEOA under visible light illumination in MeCN : $H_2O$ : TEOA (3 : 1 : 1) (Scheme 15).[170] Similar to the case shown in Scheme 13, $Fe^{III}$TCPP was reduced by the photo-induced electrons produced in g-$C_3N_4$ nanosheets up to $Fe^{0}$TCPP that reduced $CO_2$ to CO coupled with proton transfer, whereas the holes left in g-$C_3N_4$ nanosheets were reduced by TEOA.[170] A maximum rate of 6.52 mmol $g^{-1}$ in 6 h and a selectivity up to 98% for CO production have been achieved using the g-$C_3N_4$/FeTCPP heterogeneous catalyst.[170]

To further improve the catalytic performance of composite electrodes, rutile $TiO_2$ nanoparticles were employed as modifiers to enhance interfacial charge transfer between semiconducting carbon nitride nanosheets (NS–$C_3N_4$) and a catalyst (supramolecular Ru(II)–Re(I) binuclear complex (RuRe)).[171] The RuRe/$TiO_2$/NS-$C_3N_4$ hybrid photocatalyzed $CO_2$ reduction to CO with high selectivity under visible light ($\lambda$ > 400 nm) irradiation, exhibiting higher catalytic activity compared to an analogue without $TiO_2$ by a factor of 4, in terms of both the CO formation rate and the TON.[171] The enhanced photocatalytic activity was attributed mainly to the prolonged lifetime of free and/or shallowly trapped electrons generated in $TiO_2$/NS$C_3N_4$ under visible-light irradiation, as revealed by transient absorption spectroscopy.[171]

A case of metal porphyrinoid catalysis was reported in conjunction with an inorganic semiconductor photoanode, completing a full photoelectrochemical cell. The photoelectrochemical reduction of $CO_2$ was performed in a two-compartment cell composed of an FeO(OH)/$BiVO_4$/FTO photoanode and a $Co^{II}$(Ch)/MWCNT cathode, which are connected with conducting wire as an external circuit and separated by a Nafion membrane (Fig. 14).[172] A photo-driven oxidation reaction (of water) occurs at the photoanode, and the generated electrons are transported through the external circuit, being supplied as reducing equivalents to the $Co^{II}$(Ch)/MWCNT catalyst at the cathode. The photocatalytic controlled potential electrolysis of a $CO_2$-saturated aqueous solution (pH 4.6) using a photoelectrochemical cell in Fig. 14 at an applied bias voltage of −1.3 V at the cathode *versus* the photoanode resulted in the formation of CO and $H_2$ as shown in Fig. 15a, where the CO yield is significantly higher than the $H_2$ yield.[172] The maximum current efficiency for CO production for the initial 2 h was 83% at pH 4.6.[172] The amount of $O_2$ produced in the photoelectrochemical oxidation of water is one-half of the amounts of the sum of CO and $H_2$ produced in the electrochemical reduction of $CO_2$ and $H_2O$ on the cathode (Fig. 15b).[172]

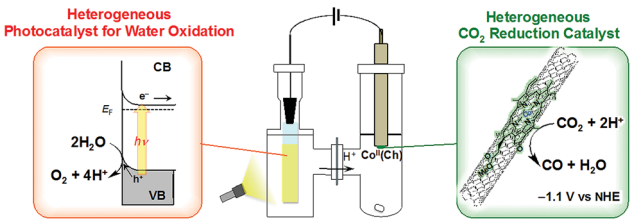


Fig. 14 Schematic illustration of a photoelectrochemical cell composed of an FeO(OH)/$BiVO_4$/FTO photoanode for the photocatalytic oxidation of water to $O_2$ and a $Co^{II}$(Ch)/MWCNT cathode for the catalytic reduction of $CO_2$ to CO. Cathode and anode compartments are separated by a Nafion membrane. Reprinted with permission from ref. 172. Copyright 2017, American Chemical Society.

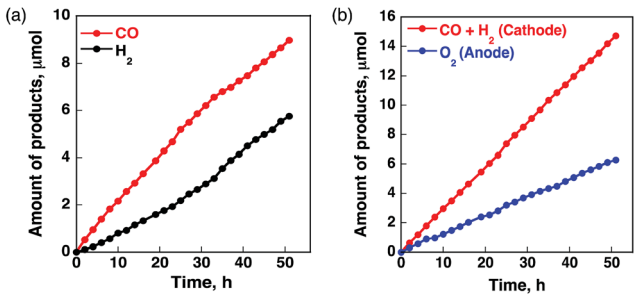


Fig. 15 Time profiles of (a) the formation of CO (red circles) and $H_2$ (black circles) and (b) the formation of $O_2$ (blue circles) and CO plus $H_2$ (red circles) in the photo-assisted CPE with the $Co^{II}$(Ch)-modified cathode at an applied bias voltage of −1.3 V at the cathode *versus* the FeO(OH)/$BiVO_4$/FTO photoanode in a $CO_2$-saturated aqueous solution containing $Na_2SO_4$ (5.0 mM) at pH 4.6 under simulated 1 sun (AM 1.5G) illumination at 298 K. Reprinted with permission from ref. 172. Copyright 2017, American Chemical Society.

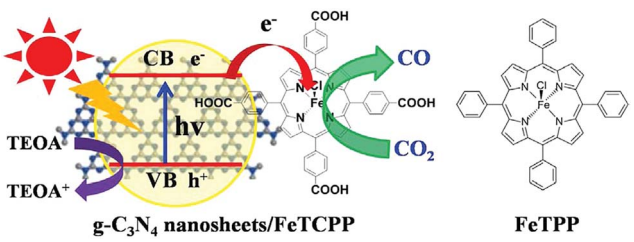


Scheme 15 Photocatalytic reduction of $CO_2$ to CO with TEOA using g-$C_3N_4$ nanosheets/FeTCPP (g-$C_3N_4$/FeTCPP). Reprinted with permission from ref. 170. Copyright 2018, Elsevier.

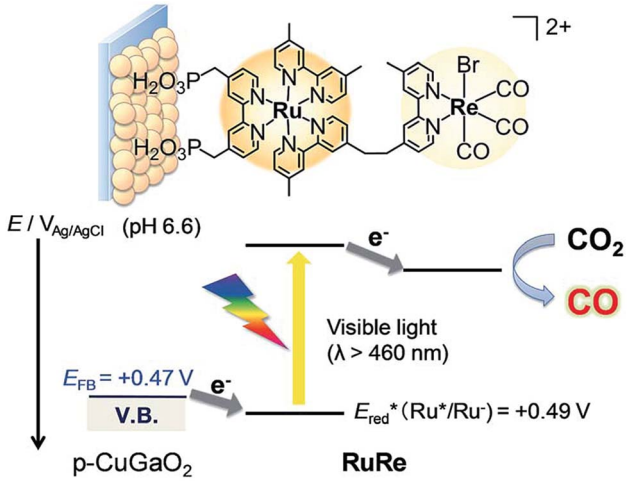


Scheme 16 Schematic illustration for the photocatalytic reduction of $CO_2$ to CO with the RuRe/$CuGaO_2$ electrode. Reprinted with permission from ref. 173. Copyright 2017, Royal Society of Chemistry.

A direct covalent linkage between a photosensitizer and a catalyst is a popular strategy due to the ease of electron transfer induced by proximity, and also one that is well suited for metal porphyrinoid catalysts owing to their synthetic versatility and flexibility. Such a case is shown in Scheme 16, where a Ru-based dye and a Re-based catalyst pair is synthesised and immobilised on a semiconductor surface. The photoelectrochemical reduction of $CO_2$ to CO was performed by using a RuRe/$CuGaO_2$ electrode under irradiation ($\lambda_{ex}$ > 460 nm), which can be selectively absorbed by the Ru photosensitizer unit of RuRe, in an aqueous solution containing $NaHCO_3$ (50 mM) saturated with $CO_2$ as shown in Scheme 16.[173] The difference in the observed current between the irradiation and dark conditions indicated that the cathodic photoresponse of the RuRe/$CuGaO_2$ electrode started at +0.30 V *vs.* Ag/AgCl (=+0.50 V *vs.* SHE), which was approximately 0.4 V more positive (due to the photovoltage supplied by the underlying semiconductor) than that of RuRe/NiO (*ca.* −0.1 V *vs.* Ag/AgCl = +0.1 *vs.* SHE).[173] The TON for the formation of CO was 125 based on the RuRe loading, and the total faradaic efficiency for the production of CO plus $H_2$ was 81%.[173] The wavelength dependence of the incident-photon-to-current efficiencies of the RuRe/$CuGaO_2$ electrode agreed well with the absorption spectrum of the electrode, whereas the $CuGaO_2$ electrode alone (without the dye and catalyst) exhibited almost no photoresponse under irradiation ($\lambda_{ex}$ > 460 nm).[173] The photocurrent was generated by the injection of the electrons from the $CuGaO_2$ electrode into the excited Ru photosensitizer unit of RuRe, as shown in Scheme 16, because the flat band potential of the $CuGaO_2$ electrode in the reaction solution (+0.47 V *vs.* Ag/AgCl = +0.67 V *vs.* SHE) is less positive than the one-electron reduction potential of the excited state of RuRe ($E_{red}$ = +0.49 V *vs.* Ag/AgCl = +0.69 V *vs.* SHE).[173]

# 8 Conclusions

The one-electron reduction of $CO_2$ to oxalic acid is catalysed not only by metalloporphyrins such as $Ag^{II}$(TPP) an $Pd^{II}$(TPP) but also by nonheme dicopper and tricopper complexes. Iron porphyrins act as efficient catalysts for both the electrocatalytic and photocatalytic reduction of $CO_2$ to CO in competition with the proton reduction to $H_2$. When four positively charged trimethylanilinium groups were introduced at the *ortho* positions of the TPP phenyls of an iron tetraphenylporphyrin (Fe-*o*-TMA in Fig. 2), the lowest overpotential of 0.220 V for $CO_2$ reduction to CO was achieved with a maximum TOF of $10^6$ $s^{-1}$. A variety of metal complexes such as cobalt and nickel complexes also act as effective catalysts for two-electron reduction of $CO_2$ to CO. When indium protoporphyrin was employed as an electrocatalyst, formate ($HCOO^-$) was the main product instead of CO and the faradaic efficiency of $HCOO^-$ at pH 9.6 was close to 70%. Whether CO or HCOOH is produced depends on the metals and ligands of metalloporphyrins.

Further reduction of CO to methane has been made possible by using a Co protoporphyrin molecular catalyst immobilized onto a pyrolytic graphite (PG) electrode (CoPP-PG) in a purely aqueous electrolyte solution. The reduction of CO to $C_2H_4$ was also made possible by using crystallized copper phthalocyanine supported on carbon black (CuPc/CB) with a maximum faradaic efficiency of 25% under atmospheric pressure at −1.4 V *vs.* SHE, while $CH_4$ and CO were produced as minor products. The photocatalytic reduction of $CO_2$ to CO occurs in competition with the proton reduction to $H_2$ using triethylamine as a reductant, $Co^{II}$(Ch)/MWCNTs as a $CO_2$ reduction catalyst, and $[Ru^{II}(Me_2phen)_3]^{2+}$ as a photosensitizer. When Fe-*p*-TMA with four positively charged trimethylanilinium groups introduced at the *para* positions of the TPP phenyls was employed as a catalyst, the photocatalytic reduction of CO using triethylamine as a reductant and Ir(ppy) afforded methane with a selectivity of up to 82% and a quantum yield of 0.18% under visible light irradiation at ambient temperature and pressure. Water can be used as an electron and proton source for the photocatalytic reduction of $CO_2$ to CO using a two-compartment cell composed of an FeO(OH)/$BiVO_4$/FTO photoanode and a $Co^{II}$(Ch)/MWCNT cathode. There are many reports on the photocatalytic reduction of $CO_2$ with water as an electron and proton source to produce CO, HCOOH and $CH_4$ using heterogeneous catalysts.[174–184] It is highly desired to develop photocatalytic systems of $CO_2$ reduction to fuels such as ethylene, methanol and methane using water as an electron and proton source using homogeneous molecular catalysts as well.

# Conflicts of interest

There are no conflicts to declare.

# Acknowledgements

The authors gratefully acknowledge the contributions of their collaborators and coworkers cited in the listed references, and support through a SENTAN project (to S. F.) from the Japan Science and Technology Agency (JST), JSPS KAKENHI (No. 16H02268 to S. F.), the NRF of Korea through CRI (NRF-2012R1A3A2048842 to W. N.), GRL (NRF-2010-00353 to W. N.), and the Basic Science Research Program

 

(2017R1D1A1B03029982 to Y. M. L., 2017R1D1A1B03032615 to S. F., and 2017R1C1B2011074 to H. S. A.).

## Notes and references

1 N. S. Lewis, *Energy Environ. Sci.*, 2016, **9**, 2172–2176.
2 M. Robert, *ACS Energy Lett.*, 2016, **1**, 281–282.
3 Y. Zeng, J. Chen, T. Yu, G. Yang and Y. Li, *ACS Energy Lett.*, 2017, **2**, 357–363.
4 J. Su and L. Vayssieres, *ACS Energy Lett.*, 2016, **1**, 121–135.
5 J. M. Thomas and K. D. M. Harris, *Energy Environ. Sci.*, 2016, **9**, 687–708.
6 N. S. Lewis, *Nat. Nanotechnol.*, 2016, **11**, 1010–1019.
7 T. A. Faunce, W. Lubitz, A. W. Rutherford, D. MacFarlane, G. F. Moore, P. Yang, D. G. Nocera, T. A. Moore, D. H. Gregory, S. Fukuzumi, K. B. Yoon, F. A. Armstrong, M. R. Wasielewski and S. Styring, *Energy Environ. Sci.*, 2013, **6**, 695–698.
8 S. Fukuzumi, *Joule*, 2017, **1**, 689–738.
9 S. Perathoner and G. Centi, *Catal. Today*, 2018, DOI: 10.1016/j.cattod.2018.03.005.
10 K. K. Sakimoto, N. Kornienko and P. Yang, *Acc. Chem. Res.*, 2017, **50**, 476–481.
11 P. V. Kamat, *Acc. Chem. Res.*, 2017, **50**, 527–531.
12 B. Wang, W. Chen, Y. Song, G. Li, W. Wei, J. Fanga and Y. Sun, *Catal. Today*, 2018, **311**, 23–39.
13 K. Maeda, *Prog. Solid State Chem.*, 2018, DOI: 10.1016/j.progsolidstchem.2017.11.003.
14 G. Zhao, X. Huang, X. Wang and X. Wang, *J. Mater. Chem.*, 2017, **5**, 21625–21649.
15 Y. Zheng, W. Zhang, Y. Li, J. Chen, B. Yu, J. Wang, L. Zhang and J. Zhang, *Nano Energy*, 2017, **40**, 512–539.
16 Y. Sohna, W. Huang and F. Taghipour, *Appl. Surf. Sci.*, 2017, **396**, 1696–1711.
17 S. R. Lingampalli, M. M. Ayyub and C. N. R. Rao, *ACS Omega*, 2017, **2**, 2740–2748.
18 X. Chang, T. Wang and J. Gong, *Energy Environ. Sci.*, 2016, **9**, 2177–2196.
19 S. Wang and X. Wang, *Small*, 2015, **11**, 3097–3112.
20 W. Kim, E. Edri and H. Frei, *Acc. Chem. Res.*, 2016, **49**, 1634–1645.
21 Y. Tamaki and O. Ishitani, *ACS Catal.*, 2017, **7**, 3394–3409.
22 J. Bonin, A. Maurin and M. Robert, *Coord. Chem. Rev.*, 2017, **334**, 184–198.
23 H. Takeda, C. Cometto, O. Ishitani and M. Robert, *ACS Catal.*, 2017, **7**, 70–88.
24 Y. Yang, S. Ajmal, X. Zheng and L. Zhang, *Sustainable Energy Fuels*, 2018, **2**, 510–537.
25 C. Genovese, C. Ampelli, S. Perathoner and G. Centi, *Green Chem.*, 2017, **19**, 2406–2415.
26 R. Francke, B. Schille and M. Roemelt, *Chem. Rev.*, 2018, **118**, 4631–4701.
27 R. Daiyan, X. Lu, T. H. Ng and R. Amal, *ChemSusChem*, 2017, **10**, 4342–4358.
28 B. Khezri, A. C. Fisher and M. Pumera, *J. Mater. Chem. A*, 2017, **5**, 8230–8246.
29 Y. Zheng, J. Wang, B. Yu, W. Zhang, J. Chen, J. Qiao and J. Zhang, *Chem. Soc. Rev.*, 2017, **46**, 1427–1463.
30 S. Ponnurangam, I. V. Chernyshova and P. Somasundaran, *Adv. Colloid Interface Sci.*, 2017, **244**, 184–198.
31 M. K. Brennaman, R. J. Dillon, L. Alibabaei, M. K. Gish, C. J. Dares, D. L. Ashford, R. L. House, G. J. Meyer, J. M. Papanikolas and T. J. Meyer, *J. Am. Chem. Soc.*, 2016, **138**, 13085–13102.
32 A. J. Martín, G. O. Larrazábal and J. Pérez-Ramírez, *Green Chem.*, 2015, **17**, 5114–5130.
33 C. Costentin, M. Robert and J.-M. Savéant, *Acc. Chem. Res.*, 2015, **48**, 2996–3006.
34 K. Mase, S. Aoi, K. Ohkubo and S. Fukuzumi, *J. Porphyrins Phthalocyanines*, 2016, **20**, 935–949.
35 J. Qiao, Y. Liu, F. Hong and J. Zhang, *Chem. Soc. Rev.*, 2014, **43**, 631–675.
36 C. Costentin, M. Robert and J.-M. Savéant, *Chem. Soc. Rev.*, 2013, **42**, 2423–2436.
37 K. Sordakis, C. Tang, L. K. Vogt, H. Junge, P. J. Dyson, M. Beller and G. Laurenczy, *Chem. Rev.*, 2018, **118**, 372–433.
38 N. Onishi, G. Laurenczy, M. Beller and Y. Himeda, *Coord. Chem. Rev.*, 2018, DOI: 10.1016/j.ccr.2017.11.021.
39 A. Álvarez, A. Bansode, A. Urakawa, A. V. Bavykina, T. A. Wezendonk, M. Makkee, J. Gascon and F. Kapteijn, *Chem. Rev.*, 2017, **117**, 9804–9838.
40 W.-H. Wang, Y. Himeda, J. T. Muckerman, G. F. Manbeck and E. Fujita, *Chem. Rev.*, 2015, **115**, 12936–12973.
41 S. Kattel, P. J. Ramírez, J. G. Chen, J. A. Rodriguez and P. Liu, *Science*, 2017, **355**, 1296–1299.
42 S. Kattel, P. Liu and J. G. Chen, *J. Am. Chem. Soc.*, 2017, **139**, 9739–9754.
43 P. Gao, S. Li, X. Bu, S. Dang, Z. Liu, H. Wang, L. Zhong, M. Qiu, C. Yang, J. Cai, W. Wei and Y. Sun, *Nat. Chem.*, 2017, **9**, 1019–1024.
44 W. H. Bernskoetter and N. Hazari, *Acc. Chem. Res.*, 2017, **50**, 1049–1058.
45 J. Klankermayer, S. Wesselbaum, K. Beydoun and W. Leitner, *Angew. Chem., Int. Ed.*, 2016, **55**, 7296–7343.
46 D. Mellmann, P. Sponholz, H. Junge and M. Beller, *Chem. Soc. Rev.*, 2016, **45**, 3954–3988.
47 A. M. Appel, J. E. Bercaw, A. B. Bocarsly, H. Dobbek, D. L. DuBois, M. Dupuis, J. G. Ferry, E. Fujita, R. Hille, P. J. A. Kenis, C. A. Kerfeld, R. H. Morris, C. H. F. Peden, A. R. Portis, S. W. Ragsdale, T. B. Rauchfuss, J. N. H. Reek, L. C. Seefeldt, R. K. Thauer and G. L. Waldrop, *Chem. Rev.*, 2013, **113**, 6621–6658.
48 S. Fukuzumi and T. Suenobu, *Dalton Trans.*, 2013, **42**, 18–28.
49 E. Fujita, J. T. Muckerman and Y. Himeda, *Biochim. Biophys. Acta*, 2013, **1827**, 1031–1038.
50 Y. Maenaka, T. Suenobu and S. Fukuzumi, *Energy Environ. Sci.*, 2012, **5**, 7360–7367.
51 S. Fukuzumi, *Eur. J. Inorg. Chem.*, 2008, 1351–1362.
52 A. J. Bard, R. Parsons and J. Jordan, *Standard potentials in aqueous solutions*, CRC press, 1985.
53 X. Huang and J. T. Groves, *Chem. Rev.*, 2018, **118**, 2491–2553.

54 P. J. Mak and I. G. Denisov, *Biochim. Biophys. Acta*, 2018, **1866**, 178–204.
55 W. Zhang, W. Lai and R. Cao, *Chem. Rev.*, 2017, **117**, 3717–3797.
56 S. Fukuzumi and W. Nam, *J. Porphyrins Phthalocyanines*, 2016, **20**, 35–44.
57 R. A. Baglia, J. P. T. Zaragoza and D. P. Goldberg, *Chem. Rev.*, 2017, **117**, 13320–13352.
58 S. Fukuzumi, T. Honda and T. Kojima, *Coord. Chem. Rev.*, 2012, **256**, 2488–2502.
59 W. Nam, *Acc. Chem. Res.*, 2015, **48**, 2415–2423.
60 X. Engelmann, I. Monte-Perez and K. Ray, *Angew. Chem., Int. Ed.*, 2016, **55**, 7632–7649.
61 G. Olivo, O. Lanzalunga and S. Di Stefano, *Adv. Synth. Catal.*, 2016, **358**, 843–863.
62 K. Ray, F. F. Pfaff, B. Wang and W. Nam, *J. Am. Chem. Soc.*, 2014, **136**, 13942–13958.
63 O. Cusso, X. Ribas and M. Costas, *Chem. Commun.*, 2015, **51**, 14285–14298.
64 Z. Chen and G. Yin, *Chem. Soc. Rev.*, 2015, **44**, 1083–1100.
65 M. Puri and L. Que Jr, *Acc. Chem. Res.*, 2015, **48**, 2443–2452.
66 P. P. Chandrachud and D. M. Jenkins, *Tetrahedron Lett.*, 2015, **56**, 2369–2376.
67 W. Nam, Y.-M. Lee and S. Fukuzumi, *Acc. Chem. Res.*, 2014, **47**, 1146–1154.
68 S. Fukuzumi, Y.-M. Lee and W. Nam, *Coord. Chem. Rev.*, 2018, **355**, 54–73.
69 S. Fukuzumi, Y.-M. Lee and W. Nam, *ChemCatChem*, 2018, **10**, 9–28.
70 S. J. C. Robinson and D. M. Heinekey, *Chem. Commun.*, 2017, **53**, 669–676.
71 J. R. McKone, S. C. Marinescu, B. S. Brunschwig, J. R. Winkler and H. B. Gray, *Chem. Sci.*, 2014, **5**, 865–878.
72 Z. Han and R. Eisenberg, *Acc. Chem. Res.*, 2014, **47**, 2537–2544.
73 V. S. Thoi, Y. Sun, J. R. Long and C. J. Chang, *Chem. Soc. Rev.*, 2013, **42**, 2388–2400.
74 E. Lamy, L. Nadjo and J. M. Savéant, *J. Electroanal. Chem.*, 1977, **78**, 403–407.
75 H. A. Schwarz and R. W. Dodson, *J. Phys. Chem.*, 1989, **93**, 409–414.
76 A. Gennaro, A. A. Isse, M.-G. Severin, E. Vianello, I. Bhugun and J.-M. Savéant, *J. Chem. Soc., Faraday Trans.*, 1996, **92**, 3963–3968.
77 J. Y. Becker, B. Vainas, R. Eger and L. Kaufman, *J. Chem. Soc., Chem. Commun.*, 1985, 1471–1472.
78 R. Angamuthu, P. Byers, M. Lutz, A. L. Spek and E. Bouwman, *Science*, 2010, **327**, 313–315.
79 J. Lan, T. Liao, T. Zhang and L. W. Chung, *Inorg. Chem.*, 2017, **56**, 6809–6819.
80 U. R. Pokharel, F. R. Fronczek and A. W. Maverick, *Nat. Commun.*, 2014, **5**, 5883.
81 B. J. Cook, G. N. Di Francesco, K. A. Abboud and L. J. Murray, *J. Am. Chem. Soc.*, 2018, **140**, 5696–5700.
82 M. Hammouche, D. Lexa, M. Momenteau and J.-M. Savéant, *J. Electroanal. Chem.*, 1988, **249**, 347–351.
83 M. Hammouche, D. Lexa, M. Momenteau and J.-M. Savéant, *J. Am. Chem. Soc.*, 1991, **113**, 8455–8466.
84 I. Bhugun, D. Lexa and J.-M. Savéant, *J. Am. Chem. Soc.*, 1994, **116**, 5015–5016.
85 B. Mondal, A. Rana, P. Sen and A. Dey, *J. Am. Chem. Soc.*, 2015, **137**, 11214–11217.
86 C. Costentin, S. Drouet, M. Robert and J.-M. Savéant, *Science*, 2012, **338**, 90–94.
87 C. Costentin, G. Passard, M. Robert and J.-M. Savéant, *J. Am. Chem. Soc.*, 2014, **136**, 11821–11829.
88 I. Azcarate, C. Costentin, M. Robert and J.-M. Savéant, *J. Am. Chem. Soc.*, 2016, **138**, 16639–16644.
89 I. Azcarate, C. Costentin, M. Robert and J.-M. Savéant, *J. Phys. Chem. C*, 2016, **120**, 28951–28960.
90 C. Costentin, M. Robert, J.-M. Savéant and A. Tatin, *Proc. Natl. Acad. Sci. U. S. A.*, 2015, **112**, 6882–6886.
91 S. Aoi, K. Mase, K. Ohkubo and S. Fukuzumi, *Chem. Commun.*, 2015, **51**, 10226–10228.
92 A. Maurin and M. Robert, *J. Am. Chem. Soc.*, 2016, **138**, 2492–2495.
93 X. Zhang, Z. Wu, X. Zhang, L. Li, Y. Li, H. Xu, X. Li, X. Yu, Z. Zhang, Y. Liang and H. Wang, *Nat. Commun.*, 2017, **8**, 14675.
94 A. Maurin and M. Robert, *Chem. Commun.*, 2016, **52**, 12084–12087.
95 Y. Wu, J. Jiang, Z. Weng, M. Wang, D. L. J. Broere, Y. Zhong, G. W. Brudvig, Z. Feng and H. Wang, *ACS Cent. Sci.*, 2017, **3**, 847–852.
96 A. Chapovetsky, T. H. Do, R. Haiges, M. K. Takase and S. C. Marinescu, *J. Am. Chem. Soc.*, 2016, **138**, 5765–5768.
97 A. Chapovetsky, M. Welborn, J. M. Luna, R. Haiges, T. F. Miller III and S. C. Marinescu, *ACS Cent. Sci.*, 2018, **4**, 397–404.
98 C. Cometto, L. Chen, P.-K. Lo, Z. Guo, K.-C. Lau, E. Anxolabéhère-Mallart, C. Fave, T.-C. Lau and M. Robert, *ACS Catal.*, 2018, **8**, 3411–3417.
99 M. D. Sampson and C. P. Kubiak, *J. Am. Chem. Soc.*, 2016, **138**, 1386–1393.
100 J. W. Raebiger, J. W. Turner, B. C. Noll, C. J. Curtis, A. Miedaner, B. Cox and D. L. DuBois, *Organometallics*, 2006, **25**, 3345–3351.
101 K.-Y. Wong, W.-H. Chung and C.-P. Lau, *J. Electroanal. Chem.*, 1998, **453**, 161–169.
102 J. M. Smieja, M. D. Sampson, K. A. Grice, E. E. Benson, J. D. Froehlich and C. P. Kubiak, *Inorg. Chem.*, 2013, **52**, 2484–2491.
103 Z. Chen, C. Chen, D. R. Weinberg, P. Kang, J. J. Concepcion, D. P. Harrison, M. S. Brookhart and T. J. Meyer, *Chem. Commun.*, 2011, **47**, 12607–12609.
104 M. D. Sampson, J. D. Froehlich, J. M. Smieja, E. E. Benson, I. D. Sharp and C. P. Kubiak, *Energy Environ. Sci.*, 2013, **6**, 3748–3755.
105 J. Agarwal, E. Fujita, H. F. Schaefer III and J. T. Muckerman, *J. Am. Chem. Soc.*, 2012, **134**, 5180–5186.
106 J. A. Keith, K. A. Grice, C. P. Kubiak and E. A. Carter, *J. Am. Chem. Soc.*, 2013, **135**, 15823–15829.

 

107 T. W. Schneider, M. Z. Ertem, J. T. Muckerman and A. M. Angeles-Boza, *ACS Catal.*, 2016, **6**, 5473–5481.
108 M. L. Clark, P. L. Cheung, M. Lessio, E. A. Carter and C. P. Kubiak, *ACS Catal.*, 2018, **8**, 2021–2029.
109 Y. C. Lam, R. J. Nielsen, H. B. Gray and W. A. Goddard III, *ACS Catal.*, 2015, **5**, 2521–2528.
110 C. Riplinger and E. A. Carter, *ACS Catal.*, 2015, **5**, 900–908.
111 K. T. Ngo, M. McKinnon, B. Mahanti, R. Narayanan, D. C. Grills, M. Z. Ertem and J. Rochford, *J. Am. Chem. Soc.*, 2017, **139**, 2604–2618.
112 J. E. Vandezande and H. F. Schaefer III, *Organometallics*, 2018, **37**, 337–342.
113 M. Bourrez, M. Orio, F. Molton, H. Vezin, C. Duboc, A. Deronzier and S. Chardon-Noblat, *Angew. Chem., Int. Ed.*, 2014, **53**, 240–243.
114 T. E. Rosser, C. D. Windle and E. Reisner, *Angew. Chem., Int. Ed.*, 2016, **55**, 7388–7392.
115 F. Li, K. Fan, B. Xu, E. Gabrielsson, Q. Daniel, L. Li and L. Sun, *J. Am. Chem. Soc.*, 2015, **137**, 9153–9159.
116 S. Sato, K. Saita, K. Sekizawa, S. Maeda and T. Morikawa, *ACS Catal.*, 2018, **8**, 4452–4458.
117 X. Su, K. M. McCardle, J. A. Panetier and J. W. Jurss, *Chem. Commun.*, 2018, **54**, 3351–3354.
118 M. Sheng, N. Jiang, S. Gustafson, B. You, D. H. Ess and Y. Sun, *Dalton Trans.*, 2015, **44**, 16247–16250.
119 J. Schneider, H. Jia, K. Kobiro, D. E. Cabelli, J. T. Muckerman and E. Fujita, *Energy Environ. Sci.*, 2012, **5**, 9502–9510.
120 M. Beley, J.-P. Collin, R. Ruppert and J.-P. Sauvage, *J. Am. Chem. Soc.*, 1986, **108**, 7461–7467.
121 M. Beley, J.-P. Collin, R. Ruppert and J.-P. Sauvage, *J. Chem. Soc., Chem. Commun.*, 1984, 1315–1316.
122 Y. Wu, B. Rudshteyn, A. Zhanaidarova, J. D. Froehlich, W. Ding, C. P. Kubiak and V. S. Batista, *ACS Catal.*, 2017, **7**, 5282–5288.
123 J. Schneider, H. Jia, J. T. Muckerman and E. Fujita, *Chem. Soc. Rev.*, 2012, **41**, 2036–2051.
124 D. C. Grills, D. E. Polyansky and E. Fujita, *ChemSusChem*, 2017, **10**, 4359–4373.
125 N. D. Loewen, T. V. Neelakantan and L. A. Berben, *Acc. Chem. Res.*, 2017, **50**, 2362–2370.
126 Y. Y. Birdja, J. Shen and M. T. M. Koper, *Catal. Today*, 2017, **288**, 37–47.
127 A. W. Nichols, S. Chatterjee, M. Sabat and C. W. Machan, *Inorg. Chem.*, 2018, **57**, 2111–2121.
128 F. Bertini, N. Gorgas, B. Stöger, M. Peruzzini, L. F. Veiros, K. Kirchner and L. Gonsalvi, *ACS Catal.*, 2016, **6**, 2889–2893.
129 C. Federsel, A. Boddien, R. Jackstell, R. Jennerjahn, P. J. Dyson, R. Scopelliti, G. Laurenczy and M. Beller, *Angew. Chem., Int. Ed.*, 2010, **49**, 9777–9780.
130 C. Ziebart, C. Federsel, P. Anbarasan, R. Jackstell, R. Baumann, W. A. Spannenberg and M. Beller, *J. Am. Chem. Soc.*, 2012, **134**, 20701–20704.
131 A. Taheri, E. J. Thompson, J. C. Fettinger and L. A. Berben, *ACS Catal.*, 2015, **5**, 7140–7151.
132 A. Taheri, N. D. Loewen, D. B. Cluff and L. A. Berben, *Organometallics*, 2018, **37**, 1087–1091.
133 S. Roy, B. Sharma, J. Pécaut, P. Simon, M. Fontecave, P. D. Tran, E. Derat and V. Artero, *J. Am. Chem. Soc.*, 2017, **139**, 3685–3696.
134 B. Reuillard, K. H. Ly, T. E. Rosser, M. F. Kuehnel, I. Zebger and E. Reisner, *J. Am. Chem. Soc.*, 2017, **139**, 14425–14435.
135 A. Sinopoli, N. T. La Porte, J. F. Martinez, M. R. Wasielewski and M. Sohail, *Coord. Chem. Rev.*, 2018, **365**, 60–74.
136 J. J. Walsh, C. L. Smith, G. Neri, G. F. S. Whitehead, C. M. Robertson and A. J. Cowan, *Faraday Discuss.*, 2015, **183**, 147–160.
137 M. Stanbury, J.-D. Compain and S. Chardon-Noblat, *Coord. Chem. Rev.*, 2018, **36**, 120–137.
138 T. Fogeron, T. K. Todorova, J.-P. Porcher, M. Gomez-Mingot, L.-M. Chamoreau, C. Mellot-Draznieks, Y. Li and M. Fontecave, *ACS Catal.*, 2018, **8**, 2030–2038.
139 Y.-E. Kim, J. Kim and Y. Lee, *Chem. Commun.*, 2014, **50**, 11458–11461.
140 C. Yoo, Y.-E. Kim and Y. Lee, *Acc. Chem. Res.*, 2018, **51**, 1144–1152.
141 J. S. Anderson, V. M. IIuc and G. L. Hillhouse, *Inorg. Chem.*, 2010, **49**, 10203–10207.
142 R. Beck, M. Shoshani, J. Krasinkiewicz, J. A. Hatnean and S. A. Johnson, *Dalton Trans.*, 2013, **42**, 1461–1475.
143 M. Aresta, C. F. Nobile, V. G. Albano, E. Forni and M. Manassero, *J. Chem. Soc., Chem. Commun.*, 1975, 636–637.
144 C. Yoo and Y. Lee, *Chem. Sci.*, 2017, **8**, 600–605.
145 C. Yoo, J. Kim and Y. Lee, *Organometallics*, 2013, **32**, 7195–7203.
146 D. Sahoo, C. Yoo and Y. Lee, *J. Am. Chem. Soc.*, 2018, **140**, 2179–2185.
147 J. Shen, R. Kortlever, R. Kas, Y. Y. Birdja, O. Diaz-Morales, Y. Kwon, I. Ledezma-Yanez, K. J. P. Schouten, G. Mul and M. T. M. Koper, *Nat. Commun.*, 2015, **6**, 8177.
148 S. Kusama, T. Saito, H. Hashiba, A. Sakai and S. Yotsuhashi, *ACS Catal.*, 2017, **7**, 8382–8385.
149 M. Gong, Z. Cao, W. Liu, E. M. Nichols, P. T. Smith, J. S. Derrick, Y.-S. Liu, J. Liu, X. Wen and C. J. Chang, *ACS Cent. Sci.*, 2017, **3**, 1032–1040.
150 S. Aoi, K. Mase, K. Ohkubo and S. Fukuzumi, *Catal. Sci. Technol.*, 2016, **6**, 4077–4080.
151 S. Aoi, K. Mase, K. Ohkubo and S. Fukuzumi, *Chem. Commun.*, 2015, **51**, 15145–15148.
152 H. Rao, L. C. Schmidt, J. Bonin and M. Robert, *Nature*, 2017, **548**, 74–77.
153 C. Steinlechner and H. Junge, *Angew. Chem., Int. Ed.*, 2018, **57**, 44–45.
154 T. Wu, L. Zou, D. Han, F. Li, Q. Zhang and L. Niu, *Green Chem.*, 2014, **16**, 2142–2146.
155 B. AlOtaibi, S. Fan, D. Wang, J. Ye and Z. Mi, *ACS Catal.*, 2015, **5**, 5342–5348.
156 X. Liu, S. Inagaki and J. Gong, *Angew. Chem., Int. Ed.*, 2016, **55**, 14924–14950.
157 Y. Wang, X. Bai, H. Qin, F. Wang, Y. Li, X. Li, S. Kang, Y. Zuo and L. Cui, *ACS Appl. Mater. Interfaces*, 2016, **8**, 17212–17219.
158 L. Yu, G. Li, X. Zhang, X. Ba, G. Shi, Y. Li, P. K. Wong, J. C. Yu and Y. Yu, *ACS Catal.*, 2016, **6**, 6444–6454.

159 H. Wang, Y. Chen, X. Hou, C. Ma and T. Tan, *Green Chem.*, 2016, **18**, 3250–3256.
160 H. Rao, J. Bonin and M. Robert, *Chem. Commun.*, 2017, **53**, 2830–2833.
161 Y. Tamaki, K. Koike, T. Morimoto and O. Ishitani, *J. Catal.*, 2013, **304**, 22–28.
162 Y. Kuramochi and O. Ishitani, *Inorg. Chem.*, 2016, **55**, 5702–5709.
163 E. Hasegawa, S. Takizawa, T. Seida, A. Yamaguchi, N. Yamaguchi, N. Chiba, T. Takahashi, H. Ikeda and K. Akiyama, *Tetrahedron*, 2006, **62**, 6581–6588.
164 Z. Guo, F. Yu, Y. Yang, C.-F. Leung, S.-M. Ng, C.-C. Ko, C. Cometto, T.-C. Lau and M. Robert, *ChemSusChem*, 2017, **10**, 4009–4013.
165 D. Hong, Y. Tsukakoshi, H. Kotani, T. Ishizuka and T. Kojima, *J. Am. Chem. Soc.*, 2017, **139**, 6538–6541.
166 W. J. Ong, L. L. Tan, Y. H. Ng, S. T. Yong and S. P. Chai, *Chem. Rev.*, 2016, **116**, 7159–7329.
167 L. Wang, R.-J. Xie, T. Suehiro, T. Takeda and N. Hirosaki, *Chem. Rev.*, 2018, **118**, 1951–2009.
168 M. Mousavi, A. Habibi-Yangjeh and S. R. Pouran, *J. Mater. Sci.: Mater. Electron.*, 2018, **29**, 1719–1747.
169 H. J. Yu, R. Shi, Y. X. Zhao, T. Bian, Y. F. Zhao, C. Zhou, G. I. N. Waterhouse, L. Z. Wu, C. H. Tung and T. R. Zhang, *Adv. Mater.*, 2017, **29**, 1605148.
170 L. Lin, C. Hou, X. Zhang, Y. Wang, Y. Chen and T. He, *Appl. Catal., B*, 2018, **221**, 312–319.
171 K. Wada, C. S. K. Ranasinghe, R. Kuriki, A. Yamakata, O. Ishitani and K. Maeda, *ACS Appl. Mater. Interfaces*, 2017, **9**, 23869–23877.
172 S. Aoi, K. Mase, K. Ohkubo, T. Suenobu and S. Fukuzumi, *ACS Energy Lett.*, 2017, **2**, 532–536.
173 H. Kumagai, G. Sahara, K. Maeda, M. Higashi, R. Abe and O. Ishitani, *Chem. Sci.*, 2017, **8**, 4242–4249.
174 K.-L. Bae, J. Kim, C. K. Lim, K. M. Nam and H. Song, *Nat. Commun.*, 2017, **8**, 1156.
175 M. Xing, Y. Zhou, C. Dong, L. Cai, L. Zeng, B. Shen, L. Pan, C. Dong, Y. Chai, J. Zhang and Y. Yin, *Nano Lett.*, 2018, **18**, 3384–3390.
176 Y. Zhaoa, Y. Weia, X. Wua, H. Zhenga, Z. Zhao, J. Liu and J. Li, *Appl. Catal., B*, 2018, **226**, 360–372.
177 S. Wanga, Y. Guan, L. Lu, Z. Shi, S. Yan and Z. Zou, *Appl. Catal., B*, 2018, **224**, 10–16.
178 R. Long, Y. Li, Y. Liu, S. Chen, X. Zheng, C. Gao, C. He, N. Chen, Z. Qi, L. Song, J. Jiang, J. Zhu and Y. Xiong, *J. Am. Chem. Soc.*, 2017, **139**, 4486–4492.
179 J. K. Stolarczyk, S. Bhattacharyya, L. Polavarapu and J. Feldmann, *ACS Catal.*, 2018, **8**, 3602–3635.
180 S. Neaţu, J. A. Maciá-Agulló, P. Concepción and H. Garcia, *J. Am. Chem. Soc.*, 2014, **136**, 15969–15976.
181 J.-C. Wang, L. Zhang, W.-X. Fang, J. Ren, Y.-Y. Li, H.-C. Yao, J.-S. Wang and Z.-J. Li, *ACS Appl. Mater. Interfaces*, 2015, **7**, 8631–8639.
182 S. Das, S. Kumar, S. Garai, R. Pochamoni, S. Paul and S. Roy, *ACS Appl. Mater. Interfaces*, 2017, **9**, 35086–35094.
183 T. Arai, S. Sato and T. Morikawa, *Energy Environ. Sci.*, 2015, **8**, 1998–2002.
184 A. Iwase, S. Yoshino, T. Takayama, Y. H. Ng, R. Amal and A. Kudo, *J. Am. Chem. Soc.*, 2016, **138**, 10260–10264.